Myricetin ameliorates cognitive impairment in 3×Tg Alzheimer's disease mice by regulating oxidative stress and tau hyperphosphorylation

Wang, Li ; Tang, Zhi ; Li, Bo ; Peng, Yaqian ; Yang, Xi ; Xiao, Yan ; Ni, Ruiqing ; Qi, Xiao-lan

DOI: https://doi.org/10.1016/j.biopha.2024.116963

Biomedicine & Pharmacotherapy 177 (2024) 116963

Contents lists available at ScienceDirect

Biomedicine & Pharmacotherapy

journal homepage: www.elsevier.com/locate/biopha

Myricetin ameliorates cognitive impairment in 3×Tg Alzheimer's disease mice by regulating oxidative stress and tau hyperphosphorylation

Li Wang [a,1], Zhi Tang [a,1], Bo Li [a], Yaqian Peng [a], Xi Yang [b], Yan Xiao [a], Ruiqing Ni [c,d,*], Xiaolan Qi [a,e,**]

[a] Key Laboratory of Endemic and Ethnic Diseases, Ministry of Education and Key Laboratory of Medical Molecular Biology of Guizhou Province, Key Laboratory of Molecular Biology of Guizhou Medical University, Guiyang, China
[b] Guiyang Healthcare Vocational University, Guizhou ERC for Medical Resources & Healthcare Products (Guizhou Engineering Research Center for Medical Resources and Healthcare Products), Guiyang, Guizhou, China
[c] Institute for Regenerative Medicine, University of Zurich, Zurich, Switzerland
[d] Institute for Biomedical Engineering, ETH Zurich & University of Zurich, Zurich, Switzerland
[e] Collaborative Innovation Center for Prevention and Control of Endemic and Ethnic Regional Diseases Constructed by the Province and Ministry, Guiyang, China

ARTICLE INFO

Keywords:
Alzheimer's disease
Myricetin
Tau
Oxidative stress
Synaptic impairment

ABSTRACT

Background: Alzheimer's disease is characterized by abnormal β-amyloid (Aβ) plaque accumulation, tau hyperphosphorylation, reactive oxidative stress, mitochondrial dysfunction and synaptic loss. Myricetin, a dietary flavonoid, has been shown to exert neuroprotective effects in vitro and in vivo. Here, we aimed to elucidate the mechanism and pathways involved in the protective effect of myricetin.

Methods: The effect of myricetin was assessed on $A\beta_{42}$ oligomer-treated neuronal SH-SY5Y cells and in 3×Tg mice. Behavioral tests were performed to assess the cognitive effects of myricetin (14 days, ip) in 3×Tg mice. The levels of beta-amyloid precursor protein (APP), synaptic and mitochondrial proteins, glycogen synthase kinase3β (GSK3β) and extracellular regulated kinase (ERK) 2 were assessed via Western blotting. Flow cytometry assays, immunofluorescence staining, and transmission electron microscopy were used to assess mitochondrial dysfunction and reactive oxidative stress.

Results: We found that, compared with control treatment, myricetin treatment improved spatial cognition and learning and memory in 3×Tg mice. Myricetin ameliorated tau phosphorylation and the reduction in pre- and postsynaptic proteins in $A\beta_{42}$ oligomer-treated neuronal SH-SY5Y cells and in 3×Tg mice. In addition, myricetin reduced reactive oxygen species generation, lipid peroxidation, and DNA oxidation, and rescued mitochondrial dysfunction via the associated GSK3β and ERK 2 signalling pathways.

Conclusions: This study provides new insight into the neuroprotective mechanism of myricetin in vitro in cell culture and in vivo in a mouse model of Alzheimer's disease.

1. Introduction

Alzheimer's disease (AD) is the most common cause of dementia and affects more than 50 million people worldwide [1,2]. AD is pathologically characterized by β-amyloid (Aβ) plaques, neurofibrillary tangles formed by hyperphosphorylated tau, and loss of neurons and synapses [3,4]. In addition, mitochondrial dysfunction and lipid peroxidation are linked to oxidative stress and reactive oxygen species (ROS) levels in neurotoxicity during the pathological development of AD [5,6]. Oxidative stress is implicated in neurodegenerative diseases such as AD and diabetes [7–9]. Acute oxidative stress is closely related to tau phosphorylation [10] and has been shown to stimulate Aβ production and aggregation, which could further lead to tau phosphorylation [11]. In turn, the accumulation of phosphorylated tau in the hippocampus has been previously shown to contribute to oxidative stress and mitochondrial structural and functional changes, forming a vicious cycle [12–15].

Among other signalling pathways, the aberrant glycogen synthase kinase 3β (GSK3β) and extracellular regulated kinase (ERK) signalling

* Correspondence to: Wagistrasse 12, 9th floor, Zurich 8952, Switzerland.
** Correspondence to: Beijing Road No.9, Guiyang 550001, China.
E-mail addresses: ruiqing.ni@uzh.ch (R. Ni), xlq@gmc.edu.cn (X.-l. Qi).
[1] These authors contributed equally to this manuscript

https://doi.org/10.1016/j.biopha.2024.116963
Received 22 April 2024; Received in revised form 13 June 2024; Accepted 15 June 2024

pathways are involved in mitochondrial dysfunction, and the dysregulation of ROS signalling has been implicated in AD [16,17]. ERK1/2 is a type of mitogen-activated protein kinase (MAPK) that belongs to the MAPK family. ERK1 and ERK2 are two major members of the ERK family that play crucial roles in cell signal transduction. ERK2 is also referred to as MAPK1. Aβ monomers, including dimers, trimers, oligomers, protofibrils, fibrils and ultimately Aβ plaques, can form several different intermediate aggregation states. Aβ oligomers are considered the most neurotoxic form of Aβ, have been reported in various AD animal models and have been biochemically identified in brain tissue samples from patients with AD [18–20]. Moreover, Aβ oligomers and tau have been shown to interact synergistically and amplify toxic effects on synapses, mitochondria and various downstream pathways [21].

The effects of dietary flavanols and their potential for modulating cognitive function and the risk of AD have gained increasing interest [22–24]. Myricetin (3,3′,4′,5′,5′,7-hexahydroxy-flavone) is a flavonoid found in many natural plants, such as bayberry [25]. Myricetin has been shown to play a critical role in various biological pharmacological activities [26–30]. Myricetin has been shown to reduce Aβ aggregation [31] and Aβ production by restricting the activity of beta-secretase 1 [32,33] and increasing the level of α-secretase to reduce Aβ production [34]. In addition, myricetin has been shown to ameliorate Aβ-induced mitochondrial impairment [35] and alleviate the response to oxidative stress when redox homeostasis is compromised in mitochondria [36,37]. A recent study showed that myricetin prevents high-molecular-weight Aβ oligomer-induced neurotoxicity through antioxidant effects [38]. Furthermore, myricetin has been shown to eliminate phosphorylated tau and alleviate tau-induced toxicity in neuronal cells [39], potentially by activating autophagy and slowing the liquid—liquid phase separation of tau [26]. The effect of myricetin on cognitive impairment has been demonstrated in $A\beta_{42}$-intoxicated rats [29,40].

In this study, we hypothesized that myricetin treatment provides cognitive improvement by ameliorating tau phosphorylation, synaptic toxicity, mitochondrial dysfunction and ROS via the GSK3β and ERK2 (MAPK1) pathways. We assessed the effect of myricetin in vitro in cell culture and in vivo in a mouse model of AD.

2. Materials and methods

2.1. Network pharmacology (NP)

First, target prediction for myricetin was conducted using SwissTargetPrediction (http://www.swisstargetprediction.ch/), SuperPred (https://prediction.charite.de/), and the BATMAN-TCM database (http://bionet.ncpsb.org.cn/batman-tcm/). Subsequently, keyword searches for 'Alzheimer disease' were performed in the GeneCards (https://www.genecards.org/) and OMIM (https://www.omim.org/) databases to obtain disease-related targets and eliminate duplicate genes. The identified targets of the drug components were mapped against the disease targets, and a Venn diagram was created to obtain the intersection genes. The drug-intersecting genes were subsequently uploaded to the String database (https://string-db.org/) for the construction of a protein—protein interaction (PPI) network. Finally, the drug–disease intersection genes were uploaded to the DAVID database (https://david.ncifcrf.gov/summary.jsp). Using DAVID 6.8, gene functions in terms of biological process (BP), cellular component (CC), and molecular function (MF) were annotated to elucidate the role of myricetin in treating AD in the context of gene functionality.

2.2. Molecular docking

The 3D structures of the small-molecule drugs were downloaded in SDF format from PubChem, the structures were imported into ChemBio3D Ultra 14.0 for energy minimization, the minimum RMS gradient was set to 0.001, and the optimized small molecules were saved in mol2 format. The optimized small molecules were imported into AutoDockTools-1.5.6 for hydrogenation, charge calculation, charge assignment, and setting of rotatable bonds, after which the products were saved in the 'pdbqt' format. The protein structures of MAPK1 (ERK2) (PDB ID: 2Y9Q), APP (PDB ID: 4PWQ), and GSK3β (PDB ID: 6V6L) were downloaded from the PDB database. Pymol 2.3.0 was used to remove protein crystal water and the original ligands, after which the protein structures were imported into AutoDocktools (v1.5.6) for hydrogenation, charge calculation, charge assignment, and specifying atom types. The protein binding sites were predicted using POCASA 1.1, and docking was conducted using AutoDock Vina 1.1.2.

2.3. Materials, reagents, and antibodies

The list and sources of materials, including chemicals, antibodies, and kits, are described in detail in Supplemental Table 1 and **Table 2**. Human SH-SY5Y cells were obtained from Procell Life Science & Technology Co., Ltd. (Wuhan, China).

Myricetin (purity ≥98.0 %) was dissolved first in cell-grade dimethyl sulfoxide (DMSO, 10 % v/v) and then further diluted with polyethylene glycol 300 (PEG300, 40 %), Tween-80 (5 %) and saline (45 %). One milligram of $A\beta_{42}$ freeze-dried powder (purity ≥95.0 %) was dissolved in 220 μL of hexafluoro-2-propanol, incubated at 37°C for 1 h, transferred to ice for 10 min and air-dried in a fume hood at room temperature for 12 h, ensuring that the hexafluoro-2-propanol volatilized completely. A polypeptide film was formed at the bottom, and the mixture was kept at −80°C. Nine microliters of cell-grade DMSO was added after the film was fully dissolved. The solution was diluted with 441 μL of F12 medium without phenol red and incubated at 4°C for 24 hours. After centrifugation for 10 min at 14000 r/min, the supernatant was transferred to a new Eppendorf tube and stored at −80°C for future use. Western blotting was first performed to validate the aggregation of Ab using a recombinant anti-$A\beta_{42}$ antibody (ab180956) (Supplemental Table 1).

2.4. Cell culture, treatment, and extracts

SH-SY5Y cells (well-characterized cellular model of AD) were grown to 80 % confluence in 6-well culture plates and maintained in Dulbecco's modified Eagle medium (DMEM; Gibco, USA) supplemented with 10 % fetal bovine serum (Gibco, USA) in a humidified incubator with 5 % CO2 at 37°C. Cells were pretreated with myricetin (5, 10, or 20 μM) for 24 h and then incubated with 10 μM $A\beta_{42}O$ for an additional 48 h. To investigate the involvement of the ERK2 and GSK3β pathways, SH-SY5Y cells were pretreated with the MAPK/ERK pathway inhibitor PD98059 (50 μM) for 30 min or the GSK3α/GSK3β inhibitor SB216763 (5 μM) for 24 h before treatment with 5 μM myricetin [41,42].

2.5. Cell viability assay

Cell viability was measured using a cell counting kit-8 (CCK-8) (MedChemExpress, USA) as previously described [43,44]. In brief, a total of 5×10^3 cells were seeded into 96-well plates. After treatment, 10 μL of CCK-8 reagent and 100 μL of medium were added to each well, and the cells were incubated for 1 h at 37°C. Next, the absorption (450 nm) of the plate was measured using a microplate reader (Bio-Rad, Hercules, USA).

2.6. Animal experiment

All animal experiments were approved by the Institutional Animal Care and Use Committee of Guizhou Medical University (approval No. 2304543). All the experiments were complied with the ARRIVE 2.0 guidelines and were performed in accordance with guidelines under the approval of the Animal Protection and Use Committee of Guizhou Medical University. Eight C57BL/6 J mice (4 M/4 F) and sixteen 3×Tg mice (8 M/8 F) were used [45–47](weight: 24.5–25.5 g, age: 10 months)

All the experimental protocols complied with the ARRIVE 2.0 guidelines. All the experimental animals were housed under a 12:12-h light-dark cycle with ad libitum access to food and water at 22°C and a humidity of 60 %. All of the animals were allowed to adapt to the environment for 1 week.

Mice were randomly assigned to three groups: the wild-type group without any processing (WT, n = 8, 4 M/4 F), the 3×Tg control group with saline (3×Tg-saline, n = 8, 4 M/4 F), and the myricetin treatment group (3×Tg-myrecetin, n = 8, 4 M/4 F). For the myricetin group, myricetin (20 mg/kg) was administered intraperitoneally (i.p.) daily for 2 weeks [48]. The same volume of saline was administered daily via the i.p. route to the saline group. Behavioral tests were subsequently performed after the myricetin treatment period. After the behavioral tests, all the mice were sacrificed under deep anaesthesia with pentobarbital sodium (50 mg/kg body weight)[49].

2.7. Behavioral testing

The Morris water maze was used to evaluate the learning and memory function of the experimental mice. A black circular pool (140 cm diameter and 50 cm height) was filled with nontoxic white water (23–25°C, containing titanium dioxide (TiO_2) to achieve opacity. The pool was divided into four equal quadrants. All the mice were trained for 4 days, after which the platform was removed. Mice were allowed 60 seconds to swim freely. All trials were video recorded, and the data were analysed via the EthoVisionXT system from Noldus Information Technology. The dependent variables used for the analysis were latency (seconds) to reach the platform for the learning trials and the number of platform crossings, latency to first cross the platform location (seconds), and velocity (cm/second) for the probe trial.

After the behavioral tests, all the mice were sacrificed under deep anaesthesia with pentobarbital sodium (50 mg/kg body weight) and transcardially perfused with PBS (pH 7.4). The brains were subsequently removed from the skull. The left hemisphere brain tissue was saved for Western blotting and for transmission electron microscopy (TEM) and stored at −80°C. The right hemisphere mouse brain tissue was fixed in 4 % paraformaldehyde in 1× PBS (pH 7.4) for 24 h and saved in 1× PBS (pH 7.4) at 4°C. For immunofluorescence staining, the fixed right brain hemisphere tissues were dehydrated using a vacuum infiltration processor (Leica ASP200S, Germany) and embedded in paraffin using an Arcadia H heated embedding workstation (Leica, Germany).

2.8. Western blotting

Next, western blotting was performed to investigate the protein levels changes in the brain tissue from three WT and three 3×Tg mice. The protein level being assessed included beta-amyloid precursor protein (APP), presynaptic proteins (SNAP25 and synaptophysin), postsynaptic proteins (PSD95); phosphorylated tau (p-TauS396, p-TauS356 and p-TauT231) and total tau (t-tau); phosphorylated ERK (p-ERK) and total ERK (t-ERK); phosphorylated GSK3β (p-GSK3β (Tyr216), and p-GSK3β (Ser9)), total GSK3β (t-GSK3β); phosphorylated tau (dynamin-related protein 1, DRP1); and fusion proteins (mitofusin-1, Mfn1; mitofusin-2, Mfn2) after treatment, as previously described [50,51]. The antibodies used are listed in Supplementary Table 1. Total proteins from SH-SY5Y cells and the hippocampus of the mouse brain were extracted with RIPA lysis buffer (Solarbio, China) containing a protease inhibitor cocktail (1:200; Sigma, USA). Equal amounts of protein per lane (20–50 μg) were loaded onto 4 %–12 % sodium dodecyl sulfate–polyacrylamide gels (Absin, China) and transferred to polyvinylidene difluoride membranes (Millipore, USA), after which the membranes were incubated in 5 % skim milk powder (weight/volume) for 2 hours at room temperature. The membranes were incubated with primary antibodies overnight at 4°C and then incubated with goat anti-mouse or goat anti-rabbit goat anti-mouse IgG (H+L), horseradish peroxidase (HRP), or goat anti-rabbit IgG (H+L) secondary antibodies and with HRP secondary antibodies (Thermo Fisher Scientific, USA). Anti-β-tubulin or anti-β-actin was used as a loading control. Each experiment was repeated at least 3 times. Immunoreactive bands were visualized using a ChemiDoc MP imaging system (Bio-Rad, USA). Band density was analysed by ImageJ software (NIH, USA).

2.9. Mitochondrial membrane potential detection by flow cytometry

A mitochondrial membrane potential assay (JC-1 detection kit, Beyotime, China) was implemented to quantify the level of polarization/depolarization of the mitochondrial membrane after treatment with myricetin and $A\beta_{42}O$ in SH-SY5Y cells. SH-SY5Y cells were treated with 10 μM carbonyl cyanide m-chlorophenyl hydrazone for 30 min as a positive control. The cells were digested and collected in 1.5 mL Eppendorf tubes after three gentle washes with phosphate-buffered saline (PBS). A total of 1×10^6 cells were added to 0.5 mL of 1× JC-1 dye (diluted with JC-1 staining buffer and purified water). After washing the cells with 1× JC-1 buffer three times, 10^4 cells from each group were examined by using a FACSVerse™ flow cytometer (BD Biosciences, USA) at excitation wavelengths of 488 and 633 nm. Fluorescence data were recorded and analysed by using Flow Jo software (BD Biosciences, USA). Each experiment was repeated at least 3 times independently.

2.10. ROS detection by flow cytometry

To measure the level of intracellular ROS in SH-SY5Y cells after treatment with myricetin and $A\beta_{42}O$, a flow cytometry assay was performed with the fluorescent probe 2,7-dichlorofluorescein diacetate (DCFH-DA; Beyotime, China). At a density of 2×10^5, SH-SY5Y cells were inoculated in 6-well cell culture plates as described earlier [49,52]. The cells were maintained in DMEM containing 10 μM DCFH-DA at 37°C for 30 min. The staining solution containing DCFH-DA was then removed. The cells were then gently washed three times with DMEM. The cell suspension was loaded into a flow-specific tube and detected by flow cytometry at excitation and emission wavelengths of 485 and 538 nm, respectively. Fluorescence was measured by BD FACSVerse™ flow cytometry (BD Biosciences, USA). FlowJo software (BD Biosciences, USA) was used to analyse the data. Each experiment was repeated at least 3 times independently.

2.11. Measurement of lipid peroxidation and DNA damage markers

The levels of 8-hydroxy-2'-deoxyguanosine (8-OHdG) and 4-hydroxynonenal (4-HNE), which are DNA damage markers, produced by lipid peroxidation after treatment with myricetin and $A\beta_{42}O$ were evaluated. SH-SY5Y cells were grown on polylysine-coated coverslips, and mouse brain sections were fixed with 4 % paraformaldehyde in PBS (pH 7.4) for 30 min at room temperature. Cells and tissues were permeabilized by treatment with 0.1 % Triton X-100 (Solarbio, China) for 5–10 min and then incubated with primary antibodies against 8-OHdG (1:200) and 4-HNE (1:200) overnight at 4°C. After the sections were washed with PBS (pH 7.4), a fluorescent secondary antibody conjugated with Alexa Fluor 488 (1:200; Thermo Fisher Scientific, USA) or Alexa Fluor 546 (1:200; Thermo Fisher Scientific, USA) was added, and the sections were incubated for 1 h. The sections were subsequently mounted with vector medium containing 4',6-diamidino-2-phenylindole (DAPI) (Vector Laboratories, USA). All the sections were examined on an Olympus confocal microscope (Olympus, Japan) with a 40×-100× objective and a constant exposure time for each marker. The experiments were repeated three times. A total of 100 cells from each group were analysed. Each experiment was repeated at least 3 times independently.

2.12. TEM

The morphology of mitochondria in neurons in the isolated hippocampal brain tissue of wild-type mice (n = 3) and 3×Tg mice (n = 3) was

assessed by using TEM. The mouse brain tissue was pre-fixed with 3 % glutaraldehyde and post-fixed with 1 % osmium tetroxide. Next, the sample was dehydrated gradually in a series of acetone solutions with concentrations of 30 %, 50 %, 70 %, 80 %, 90 %, 95 %, and 100 %, with three changes of 100 % acetone. Dehydration and embedding were performed using a mixture of dehydration agents and Epon812 embedding agent in ratios of 3:1, 1:1, and 1:3, respectively, followed by embedding in Epon812 resin. Ultra-thin sections of approximately 60–90 nm were prepared using an ultra-microtome, mounted on copper grids, and stained. The staining process involved uranyl acetate staining for 10–15 minutes followed by lead citrate staining for 1–2 minutes at room temperature. Finally, the samples were observed using a JEM-1400FLASH transmission electron microscope (JEOL Ltd., Japan). Each copper grid was initially observed at 6000x magnification, and images were captured of selected regions of interest to observe specific pathological changes.

2.13. Statistical analysis

All analyses were performed with SPSS software, version 25.0 (IBM, USA) and GraphPad Prism version 9.0 (GraphPad, USA). The data are presented as the mean ± standard error (SD). One hundred cells from each group were analysed. Statistical significance was determined by one-way ANOVA followed by Tukey's multiple comparison test. A p value <0.05 was considered to indicate statistical significance.

3. Results

3.1. Identification of targets associated with myricetin and AD and potential molecular docking for target screening

First, the intersection of drug-target genes and AD-associated target genes was taken. A set of 199 intersecting genes related to both AD and drugs was obtained. These genes represent potential interactive target genes for the treatment of AD (Fig. 1**a**). The resulting 199 intersecting target genes were subsequently imported into the String database (https://string-db.org/) for protein—protein interaction prediction. After topological analysis of the network was conducted, degree values were used to determine the size and color of the nodes, and combined score values were used to represent the thickness of the edges. The core targets were selected to construct a PPI network through Cytoscape 3.8.2 (Fig. 1**b**). The DAVID database was used for KEGG pathway analysis. In total, 156 pathways related to the treatment of AD and 136 pathways were selected for myricetin-related disease based on $P < 0.01$, filtering out pathways associated with AD. The top 20 KEGG metabolic pathways were visualized in a bubble chart based on P values (Fig. 1**c**). Based on the preexperimental results, we conducted molecular docking analysis of the three selected targets: APP, ERK1/2 (MAPK1), and GSK3β. (d, e) 3D and 2D images of myricetin binding to APP; the binding energy was −7.0 kcal/mol indicating a favorable binding interaction. Myricetin formed hydrogen bonds with ASP-125 and ARG-116 of APP, with hydrogen bond lengths of 2.8 Å and 2.1 Å, respectively. These residues might serve as key residues for the interaction between small molecules and proteins. 3D and 2D images of the binding of myricetin to GSK3β were obtained, and a binding energy of −8.2 kcal/mol was obtained (Fig. 1**f, g**). Myricetin formed hydrogen bonds with LYS-85, ASP-200, and GLN-185 of GSK3B, with hydrogen bond lengths of 2.1 Å, 2.4 Å, and 2.4 Å, respectively. These residues may serve as key residues for the interaction between small molecules and proteins. 3D and 2D images of myricetin binding to ERK2 (MAPK1), which produced a binding energy of −8.9 kcal/mol (Fig. 1**h, i**). Myricetin formed hydrogen bonds with ASP-167, LYS-114 and MET-108 of MAPK1, and the length of hydrogen bonds are 2.5 A, 2.4 A and 2.8 A, respectively. These residues may be the key residues in the interaction between small molecules and proteins. Favorable binding effects of these three targets with myricetin were observed.

3.2. Dose—response analysis of myricetin and $A\beta_{42}O$

First, we determined the cytotoxicity and optimal dosage of myricetin (1–200 μM) and $A\beta_{42}O$ (1–60 μM) using the CCK-8 cell viability test in SH-SY5Y cells. No loss of cell viability was observed in the SH-SY5Y cells treated for 24 h with 1 μM to 15 μM myricetin compared to the control cells treated without myricetin. A dose-dependent decrease in SH-SY5Y cell viability was observed after treatment with 20–200 μM myricetin (20–70 %) (treated vs. control group) (Fig. 2**a, b**). Thus, concentrations of 5, 10, and 20 μM myricetin were selected for the following investigations. Oligomeric $A\beta_{42}$ ($A\beta_{42}O$, estimated mass 10–72 kDa) was the major species and included 16-mers, tetramers, tremers, dimers and monomers (Fig. 2**c**). Treatment with $A\beta_{42}O$ reduced cell viability from 7.5 to 60 μM by 10–30 % (Fig. 2**d**). Thus, a concentration of 10 μM $A\beta_{42}O$ was selected for subsequent investigations.

3.3. Myricetin improved spatial cognition, learning, and memory in 3×Tg mice

Next we evaluate the effect of myricetin treatment on rescuing the cognitive impairment and pathology development in the brain of 3×Tg mice. The mice were randomly divided into three groups, 3×Tg-saline, 3×Tg-myricetin and C57/BL6 group (n = 8 mice/group). Based on our results from the cell line as well as the effective and safe dose of myricetin (without cellular toxicity) in a previous study [53], we chose the 2 weeks of 20 mg/kg daily i.p. treatment scheme. No weight loss was observed in the 3×Tg mice after 2 weeks of myricetin (20 mg/kg i.p. daily) treatment or saline treatment. We assessed the spatial learning and memory function of the 3×Tg mice after 2 weeks of saline or myricintin treatment as well as in C57/BL6 mice using the Morris water maze test (Fig. 3**a**). During days 1–3 of the 4-day Morris water maze test, the latency to reach the target did not significantly differ among the groups ($p > 0.05$, 3×Tg-myricetin (20 mg/kg) vs. 3×Tg-saline group). On day 4, the latency to reach the target was lower in the myricetin-treated 3×Tg mice (20 mg/kg) than in the saline-treated 3×Tg mice ($p<0.0001$) (Fig. 3**b**). On day 5, the time spent in the target zone, number of target crossings, and distance from the target overall increased by approximately 50 % in the myricetin-treated 3×Tg mice (20 mg/kg) compared to the saline-treated 3×Tg mice ($p<0.0001$, $p=0.0008$, $p=0.0002$, respectively) (Fig. 3**c, d, g**). A representative diagram of the behavioral trajectories of the three groups on day 5 is displayed in Fig. 3**e**. The latency of the 1st entrance to the target was approximately half that of the myricetin-treated 3×Tg mice (20 mg/kg) compared to that of the saline-treated 3×Tg mice ($p<0.0001$) (Fig. 3**f**). No differences were observed among the three groups in terms of mean speed ($p<0.05$) (Fig. 3**h**).

3.4. Myricetin prevented $A\beta_{42}O$-induced tau hyperphosphorylation in SH-SY5Y cells and in 3×Tg mice

Next, we assessed the influence of myricetin (5–20 μM) treatment on the $A\beta_{42}O$ (10 μM)-induced effect on tau phosphorylation in SH-SY5Y cells. We found no change in the t-tau level in any groups that treated using varying concentration of myricetin (5–20 μM, Fig. 2**g, h**). Treatment with $A\beta_{42}O$ increased the relative expression of p-tau/t-tau (TauS396/Tau5) by 43 % ($p=0.0328$, control vs. the $A\beta_{42}O$ group; Fig. 2**g, i**), which was prevented by myricetin (5 μM, $p=0.0232$; 10 μM, $p=0.0420$; myricetin+ $A\beta_{42}O$ vs. the $A\beta_{42}O$ group) (Fig. 2**g, i**). Additionally, we observed a reduction in the precursor of APP following intervention with myricetin (5 μM) (Fig. 2**e, f**).

We further assessed the alterations in the level of tau hyperphosphorylation induced by myricetin treatment in the brain tissue from 3×Tg mice. We evaluated the changes at three tau phosphoepitopes, p-TauS396, p-TauS356 and p-TauT231 by using Western blotting, respectively. We observed that myricetin treatment suppressed hyperphosphorylation of p-TauS396, p-TauS356 and p-TauT231 in 3×Tg mice

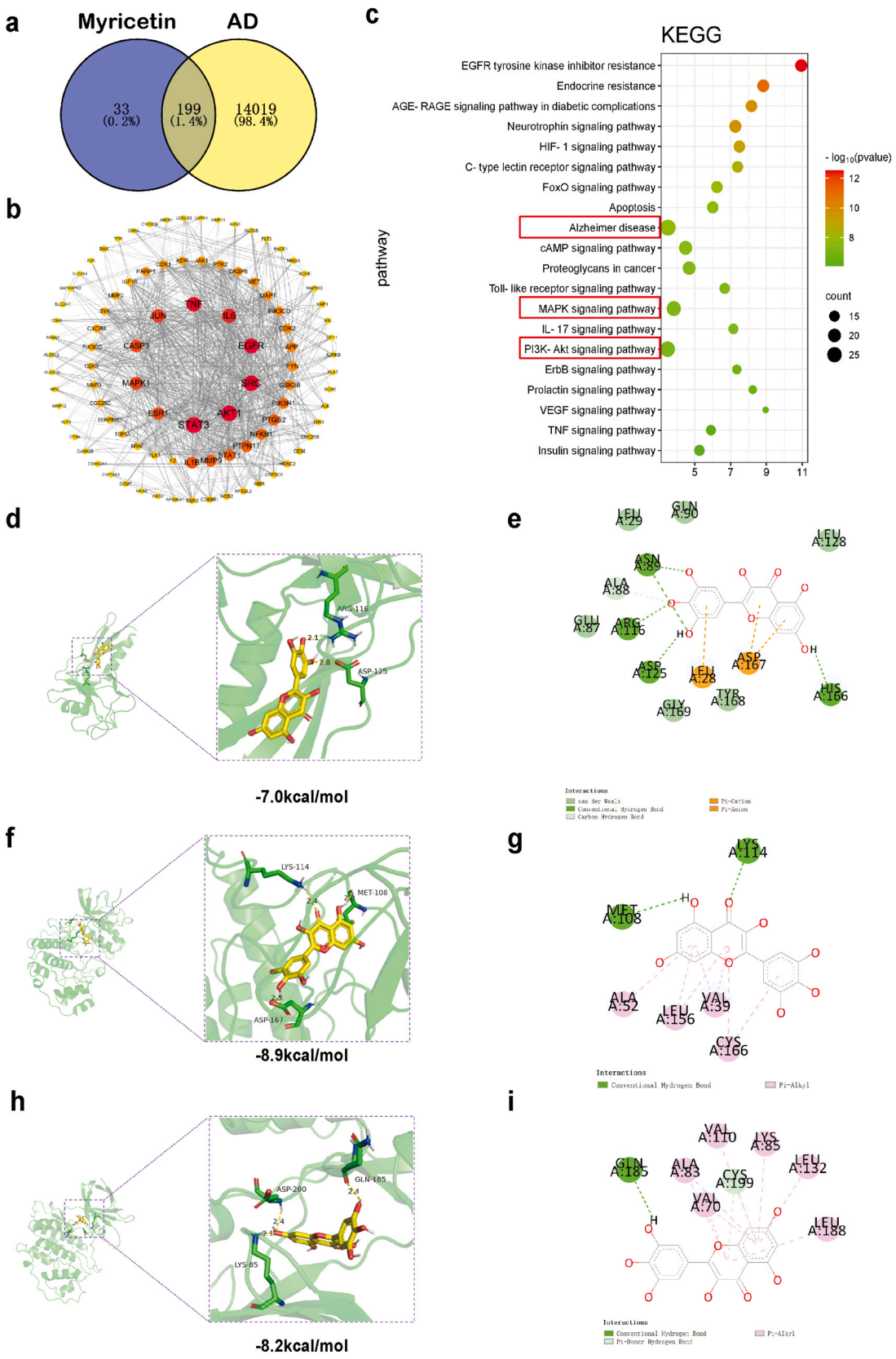

Fig. 1. In network pharmacology, myricetin was found to target the activation of Alzheimer's disease, the P38 MAPK pathway and the PI3K/AKT pathway.(a-c) Network pharmacology results of action of myricetin in AD. **(a)** Drug-disease related targets. (**b**) Core targets and network interactions. (**c**) KEGG enrichment analysis of treatment-related AD targets. (**d, e**) 3D and 2D images of the molecular docking of myricetin and APP. (**f, g**) 3D and 2D images of the molecular docking of myricetin and ERK (MAPK1). (**h, i**) 3D and 2D images of the molecular docking of myricetin and GSK3β.

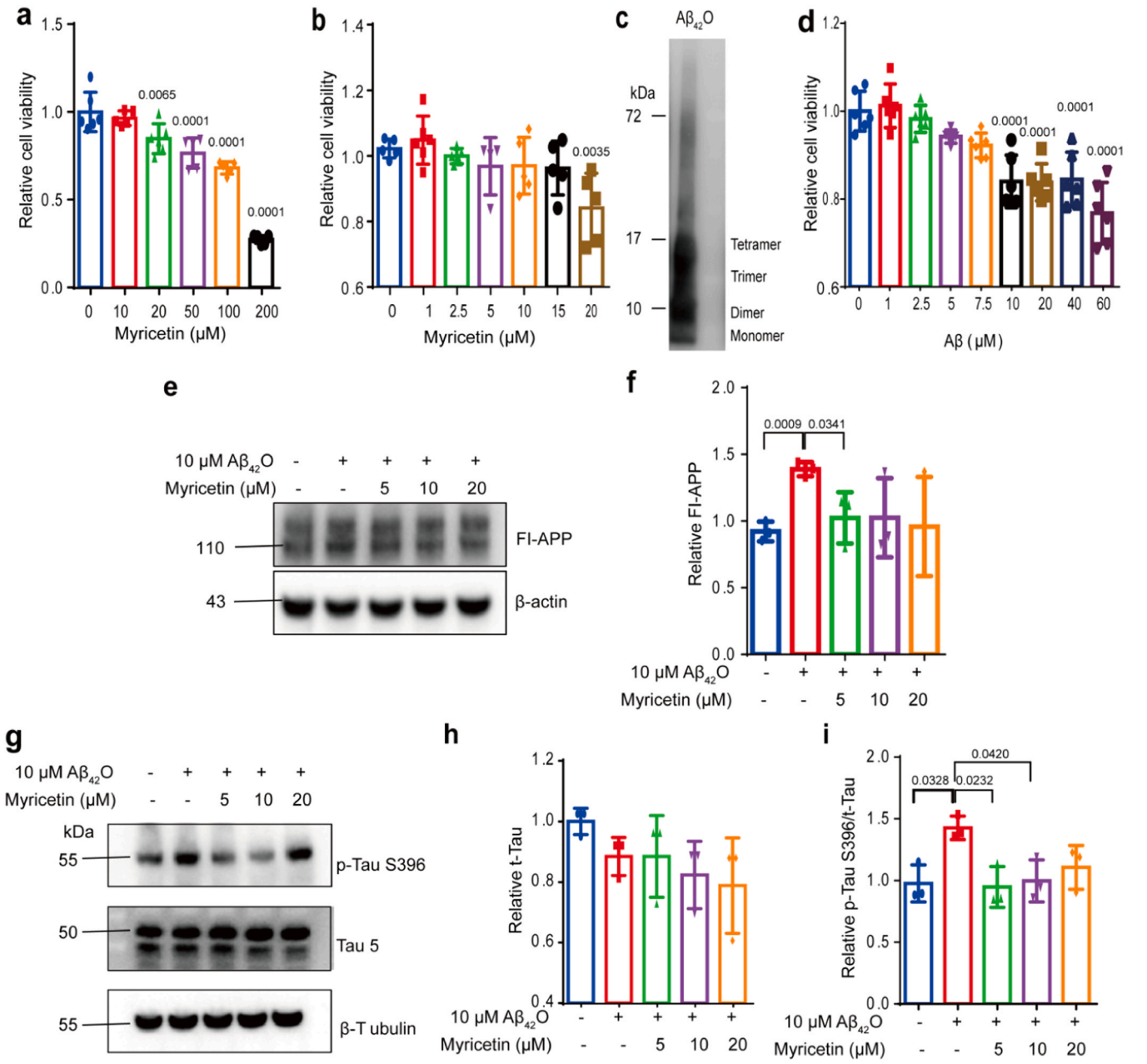

Fig. 2. Myricetin decreased Aβ$_{42}$O-induced tau phosphorylation in SH-SY5Y cells. (a, b, d) Dose—response to myricetin and Aβ$_{42}$O was assessed by using the CCK—8 assay. SH-SY5Y cells were treated without or with myricetin or Aβ$_{42}$O at different concentrations for 24 h (n=6). The data are presented as the mean ± SD. One-way ANOVA and Dunnett's multiple comparison test were used. **(c, e, g)** Representative blots of Aβ$_{42}$O, beta-amyloid precursor protein (APP), TauS396 and total tau (Tau5); (**f**) APP levels remained stable after the different treatments. (**h**) Tau5 levels remained stable after different treatments. (**i**) Myricetin decreased the Aβ$_{42}$O-induced increase in the p-TauS396/Tau5 ratio. The values were normalized to those of the control. The data are presented as the means ± SD; one-way ANOVA and Tukey's multiple comparison test were used.

(p=0.0341, p=0.0067, p=0.0454, 3×Tg-myricetin (20 mg/kg) vs. 3×Tg-saline group; Fig. 3i, k, l, m). No difference was observed in the total Tau level (Tau5) between the 3×Tg-myricetin (20 mg/kg) and 3×Tg-saline groups (p>0.05; Fig. 3**i, j**).

3.5. Myricetin ameliorated Aβ$_{42}$O-induced synaptic impairment in SH-SY5Y cells and in 3×Tg mice

Next, the influence of treatment with myricetin (5–20 μM) on the Aβ$_{42}$O (10 μM)-induced effect on synaptic impairment in SH-SY5Y cells was assessed. Treatment with Aβ$_{42}$O reduced the relative expression of the presynaptic proteins SNAP25 (by 32 %) and synaptophysin (by 23 %) and the postsynaptic protein PSD95 (by 17 %, p=0.0146 control vs. Aβ$_{42}$O group; Fig. 4**a-d**). Treatment with myricetin completely prevented this Aβ$_{42}$O-induced reduction in presynaptic SNAP25 expression (10 μM, p=0.0496; myricetin+Aβ$_{42}$O vs. Aβ$_{42}$O group) (Fig. 4**a, b**) and synaptophysin expression in SH-SY5Y cells (5 μM, p=0.0071; myricetin+Aβ$_{42}$O vs. Aβ$_{42}$O group) (Fig. 4**a, c**). Treatment with myricetin (at 5 and 10 μM) ameliorated the Aβ$_{42}$O (10 μM)-induced reduction in PSD95 expression in SH-SY5Y cells (Fig. 4**a, d**).

Subsequently, the effect of treatment with myricetin on synaptic impairment was evaluated in vivo. Myricetin treatment (20 mg/kg, i.p.) increased presynaptic SNAP25 expression (p=0.0210, 3×Tg-myricetin group vs. 3×Tg-saline group) (Fig. 5**a, b**) and synaptophysin expression in the hippocampus of 3×Tg mice (p=0.0331, 3×Tg-myricetin group vs. 3×Tg-saline group) (Fig. 5**a, c**). In addition, myricetin treatment

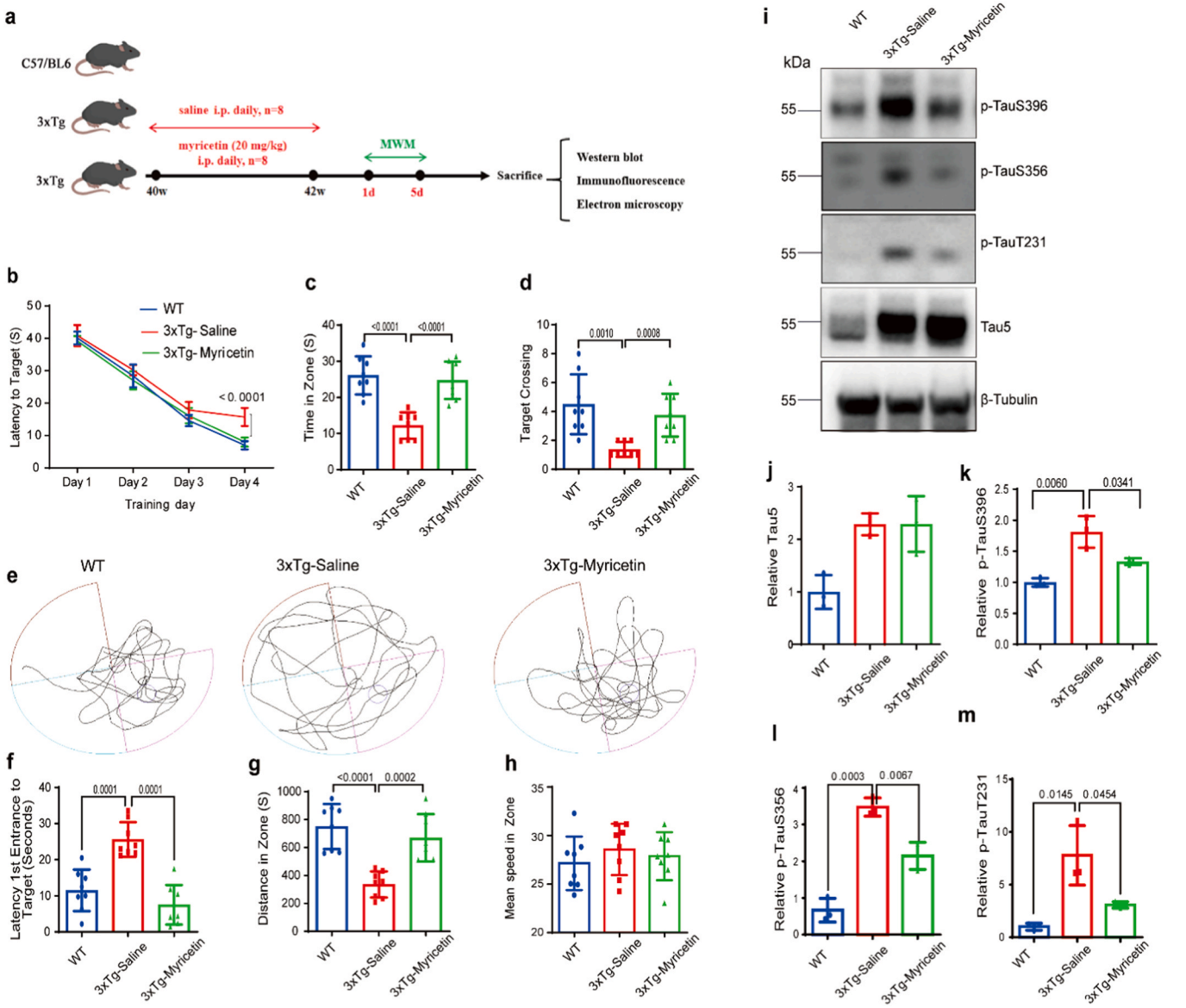

Fig. 3. Myricetin improved spatial cognition, learning, and memory in 3×Tg mice. **(a)** The experimental flowchart. The mice were randomly divided into three groups (n = 8 each). **(b-d)** Differences in the latency of the target on training days. time in zone and target crossing between groups; **(e)** Typical path tracking of mice in the Morris water maze (MWM) and probe test (without the platform). **(f)** Latency of the 1st entrance to the target without the platform. **(g)** Distance in zone within the hidden platform. **(h)** Mean speed in the zone on the fifth day. **(i)** Representative blots of TauS396, TauS356, TauT231 and total tau (Tau5). **(j, k, l, m)** Myricetin decreased the expression of p-TauS396 TauS356 and TauT231. Myricetin prevented tau phosphorylation in 3×Tg mice. There was no difference in the expression of Tau5 in myricetin group. The values were normalized to those of the wild-type group.

(20 mg/kg) restored PSD95 expression in the hippocampus of 3×Tg mice (p=0.0437, 3×Tg-myricetin vs. 3×Tg-saline group) (Fig. 5**a, d**).

3.6. Myricetin alleviated the phosphorylation of ERK2 and GSK3β in SH-SY5Y cells and in 3×Tg mice

We hypothesized that the ERK2 and GSK3β signalling pathways are involved in the neuroprotective effects of myricetin on $A\beta_{42}O$-induced alterations. Thus we assessed the influence of myricetin treatment on the effects of $A\beta_{42}O$ on p-ERK, t-ERK, p-GSK3β (Tyr216) and t-GSK3β in SH-SY5Y cells. We found no change in the t-ERK or t-GSK3β levels in any of the groups which were treated with different concentration of myricetin (5, 10, 20 μM, Fig. 4**e, f, h, i**). Intervention with $A\beta_{42}O$ (10 μM) elevated the relative expression of p-ERK/t-ERK and p-GSK3β (Tyr216) /t-GSK3β (by 165 % p=0.0008, 58 %, p=0.0261 control vs. $A\beta_{42}O$ group). Treatment with myricetin at various concentration prevented this $A\beta_{42}O$ (10 μM)-induced increase in p-ERK1/2 (5 μM p=0.0002, 10 μM p=0.0172, 20 μM p=0.0038, control vs. $A\beta_{42}O$ group). Treatment with myricetin only shown a significant reduction effect on $A\beta_{42}O$ (10 μM)-induced increase in p-GSK3β (Tyr216) at 5 μM (p=0.0253, control vs. $A\beta_{42}O$ group) but not at 10 μM or 20 μM (Fig. 4**e, g, h, j**).

In the following in vivo studies, we found that intervention with myricetin (20 mg/kg) effectively decreased the expression of p-ERK (p=0.0388, 3×Tg-myricetin vs. 3×Tg-saline group). We evaluated the alterations at three GSK3β phosphoepitopes, including an inactive form p-GSK3β Ser9, and an active form p-GSK3β Tyr216. We found the levels of p-GSK3β Tyr216 was reduced (p=0.0085) while p-GSK3β Ser9 was increased (p=0.0284) in 3×Tg-myricetin group compared to 3×Tg-saline group after treatment with myricetin (20 mg/kg) (Fig. 5**e, g, h, j**). There was no alteration in the levels of t-ERK or t-GSK3β in the 3×Tg-myricetin or 3×Tg-Saline group after treatment with myricetin (20 mg/kg) (Fig. 5**e, f, h, i**).

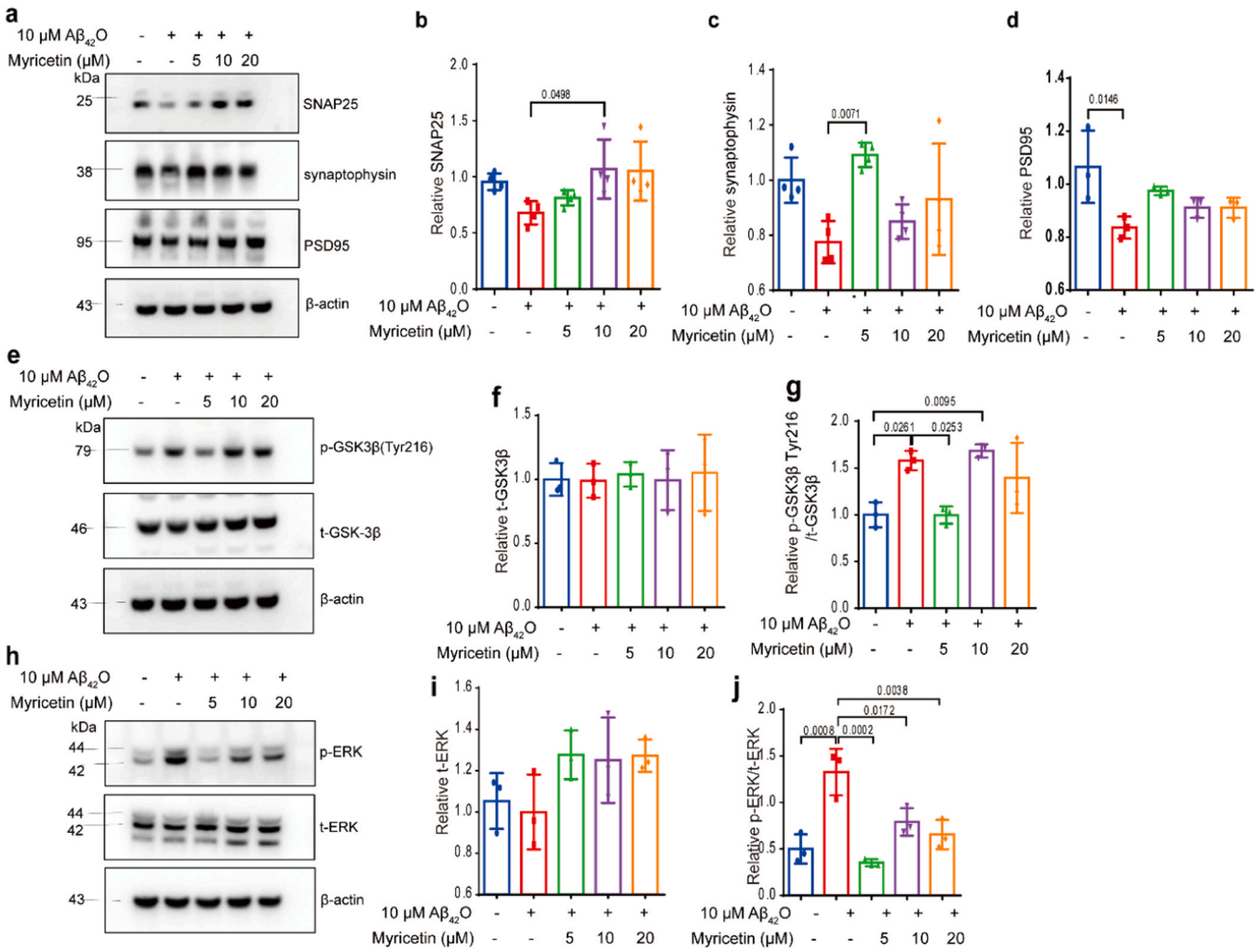

Fig. 4. Myricetin enhanced the Aβ$_{42}$O-induced reduction in the expression of synaptic proteins and attenuated p-GSK3β and p-ERK2 expression in SH-SY5Y cells. (**a-d**) Representative blots and quantification of the expression of (**a-d**) presynaptic SNAP25, synaptophysin, and postsynaptic PSD95. (**e-g**) t-ERK and p-ERK (n=3), (**h-j**) t-GSK3β and p-GSK3β(Tyr216)//t-GSK3β. The values were normalized to those of the control. The representative membranes were incubated with synaptic-associated protein antibodies (SNAP25, synaptophysin, and postsynaptic PSD95), cleaned with membrane regeneration solution and reincubated with antibodies against t-ERK and p-ERK. The same loading control was used in 4a and e. The data are presented as the mean ± SD; one-way ANOVA and Tukey's multiple comparison test were used.

Considering the potential indirect involvement of the ERK2 and GSK3β signalling pathways, we employed specific inhibitors to assess pathway-specific participation. PD98059 is a selective and potent MAPK1 (ERK2) signalling inhibitor. Treatment with 50 μM PD98059 significantly inhibited the expression of p-ERK, similar to the consistent induction by 5 μM myricetin ($p = 0.0096$; Fig. 5**a, c**), but had no significant effect on the t-ERK level in SH-SY5Y cells (Fig. 6**a, b**). Treatment with 50 μM PD98059 further decreased the level of p-GSK3β Tyr216 induced by 5 μM myricetin ($p = 0.0451$; Fig. 6**a, e**) without impacting the level of t-GSK3β in SH-SY5Y cells (Fig. 6**a, d**).

SB216732 is an inhibitor of both GSK3α and GSK3β. Treatment with 5 μM SB216763 decreased the level of p-ERK induced by 5 μM myricetin ($p = 0.0292$; Fig. 6**f, h**) without affecting the level of t-ERK in SH-SY5Y cells (Fig. 6**f, g**). Treatment with 5 μM SB216763 further reduced the level of p-GSK3β Tyr216 induced by 5 μM myricetin ($p < 0.0001$; Fig. 6**f, j**) without influencing the level of t-GSK3β in SH-SY5Y cells (Fig. 6**f, i**).

3.7. Myricetin restored mitochondrial fission protein, mitochondrial membrane potential reduction and DRP1 phosphorylation in SH-SY5Y cells and in 3×Tg mice

Next, we assessed the influence of myricetin treatment (5, 10, 20 μM) on the effect of Aβ$_{42}$O on mitochondrial function in SH-SY5Y cells. Treatment with Aβ$_{42}$O (10 μM) reduced the relative expression of the mitochondrial fission proteins Mfn1 (by 43 %) and Mfn2 (by 30 %) ($p=0.0309$ and $p=0.0004$, control vs. Aβ$_{42}$O group). Myricetin treatment reversed the Aβ$_{42}$O-induced decreases in Mfn1 expression (10 μM, $p=0.0353$; 20 μM $p=0.0198$, myricetin+Aβ$_{42}$O vs. Aβ$_{42}$O group) and Mfn2 expression (5 μM, $p=0.008$; 10 μM, $p=0.003$; 20 μM, $p=0.0027$; myricetin+Aβ$_{42}$O vs. Aβ$_{42}$O group) (Fig. 7a, b, c). We found no change in the t-DRP1 level in any of the groups, however an increase was observed in the the relative expression of p-DRP1/t-DRP1 by 33 % in the Aβ$_{42}$O group ($p=0.0190$, vs. control group). Treatment with myricetin (5 μM but not 10 μM) prevented this Aβ$_{42}$O-induced increase in p-DRP1/t-DRP1 expression in SH-SY5Y cells ($p=0.0386$, myricetin+Aβ$_{42}$O vs. Aβ$_{42}$O group) (Fig. 7a, d, e).

In vivo, myricetin treatment for 2 weeks (20 mg/kg, i.p.) reversed the decreases in the expression of Mfn1 ($p=0.0011$) and Mfn2 ($p=0.0435$) in the hippocampi of 3×Tg mice (3×Tg-myricetin vs. 3×Tg-saline group) (Fig. 8**a, b, c**). In addition, we found that myricetin treatment (20 mg/kg) could reverse the increase in the expression of p-DRP1/t-DRP1 in the hippocampus of 3×Tg mice ($p=0.0283$, 3×Tg-myricetin vs. 3×Tg-saline groups).

TEM images of mitochondrial structures revealed altered

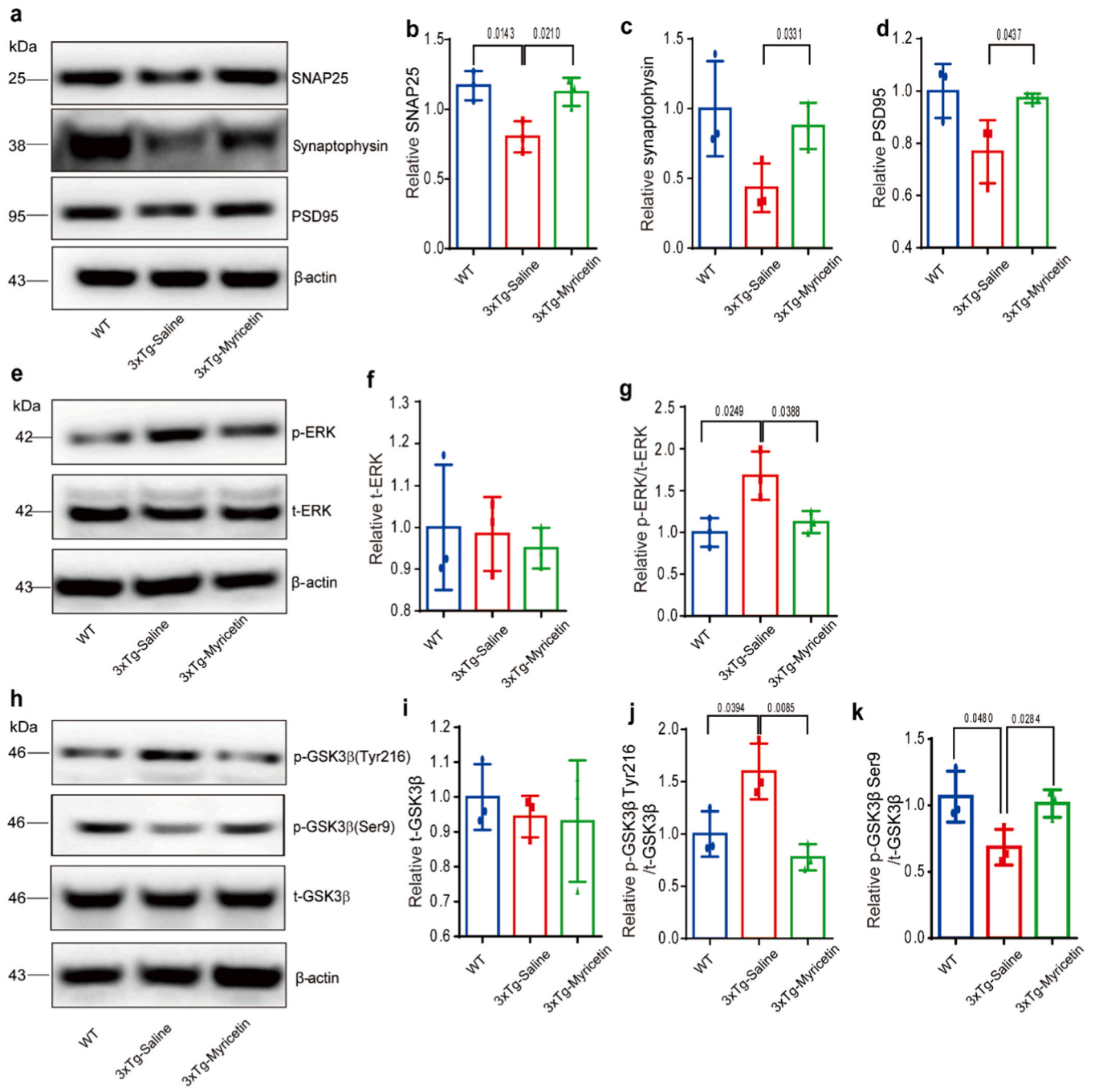

Fig. 5. Myricetin enhanced the reduction in synaptic protein expression and attenuated p-GSK3β and p-ERK2 expression in 3×Tg mice. Representative blots and quantification of the expression of (**a-d**) presynaptic SNAP25, synaptophysin, and postsynaptic PSD95; (**e-g**) t-ERK and p-ERK; and (**h-k**) t-GSK3β, p-GSK3β (Tyr216)/t-GSK3β, p-GSK3β (Ser9)/t-GSK3β (n=3 per group). The values were normalized to those of the control. The representative membranes were incubated with synaptic-associated protein antibodies (SNAP25, synaptophysin, and postsynaptic PSD95), cleaned with membrane regeneration solution and reincubated with antibodies against t-ERK and p-ERK. The data are presented as the mean ± SD; one-way ANOVA and Tukey's multiple comparison test were used.

mitochondrial morphology in neurons from the hippocampus of 3×Tg mice. We found that myricetin treatment (20 mg/kg) reversed the changes in mitochondrial morphology in the hippocampi of 3×Tg mice: the increase in mitochondrial fragmentation, indicated by the appearance of small and punctate mitochondria, was lower in the 3×Tg-myricetin group than in the 3×Tg-saline group (Fig. 8**f**). The mitochondrial perimeter of 3×Tg-saline group was significantly larger than that of 3×Tg-myricetin group ($p=0.0382$, 3×Tg-myricetin vs. 3×Tg-saline) and WT group ($p=0.0014$, 3×Tg-myricetin vs. WT). Additionally, the mitochondrial damage rate was significantly increase in the 3×Tg-saline group compared to the myricetin-treated 3×Tg group ($p<0.0001$, 3×Tg-myricetin vs. 3×Tg-saline) and WT group ($p=0.0010$, 3×Tg-myricetin vs. WT).

Next we examined the effect of myricetin on the $A\beta_{42}O$-induced alteration in the ΔΨm by using flow cytometry. When Ψm is decreased, JC-1 aggregates (emitting red fluorescence) are converted to the monomeric state, emitting green fluorescence. We found that treatment with $A\beta_{42}O$ (10 μM) increased the ratio of green/red fluorescence, indicative of the monomer/J-aggregate ratio, by 272 % ($p<0.0001$, control vs. $A\beta_{42}O$ group; Fig. 7**f, k**). Treatment with myricetin (5, 10, 20 μM) prevented this $A\beta_{42}O$-induced increase in the monomer/J-aggregate ratio in SH-SY5Y cells ($p<0.0001$ for all three conditions 5,

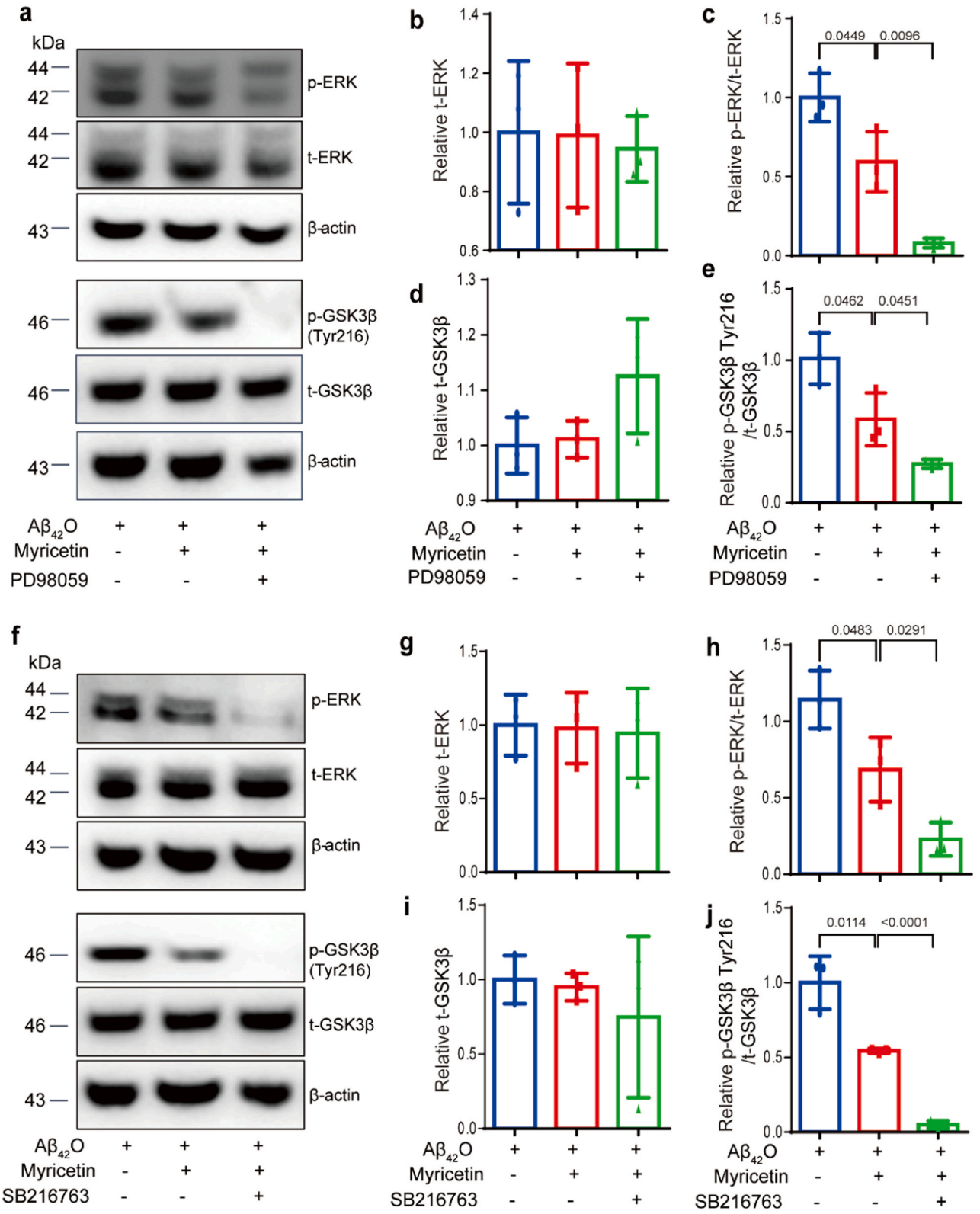

Fig. 6. Effect of myricetin on Aβ$_{42}$O-induced SH-SY5Y cells treated with a selective ERK inhibitor and a GSK3α/GSK3β inhibitor. (**a-e**) Representative blots and quantification of the levels of t-ERK, p-ERK/t-ERK, t-GSK3β and p-GSK3β(Tyr216)/t-GSK3β under the influence of an ERK1/2 inhibitor (PD98059). (**b, c**) t-ERK, p-ERK/t-ERK, (**d, e**) t-GSK3β and p-GSK3β(Tyr216)/t-GSK3β (n=3 per group). (**f-j**) Representative blots and quantification of the levels of t-ERK, p-ERK(Tyr216)/t-ERK, t-GSK3β and p-GSK3β(Tyr216)/t-GSK3β, under the influence of a GSK3α/GSK3β inhibitor (SB216763). (**g, h**) t-ERK, and p-ERK(Tyr216)/t-ERK, (**i, j**) t-GSK3β and p-GSK3β(Tyr216)/t-GSK3β (n=3 per group). The values were normalized to those of the control. The data are presented as the mean ± SD; one-way ANOVA and Tukey's multiple comparison test were used.

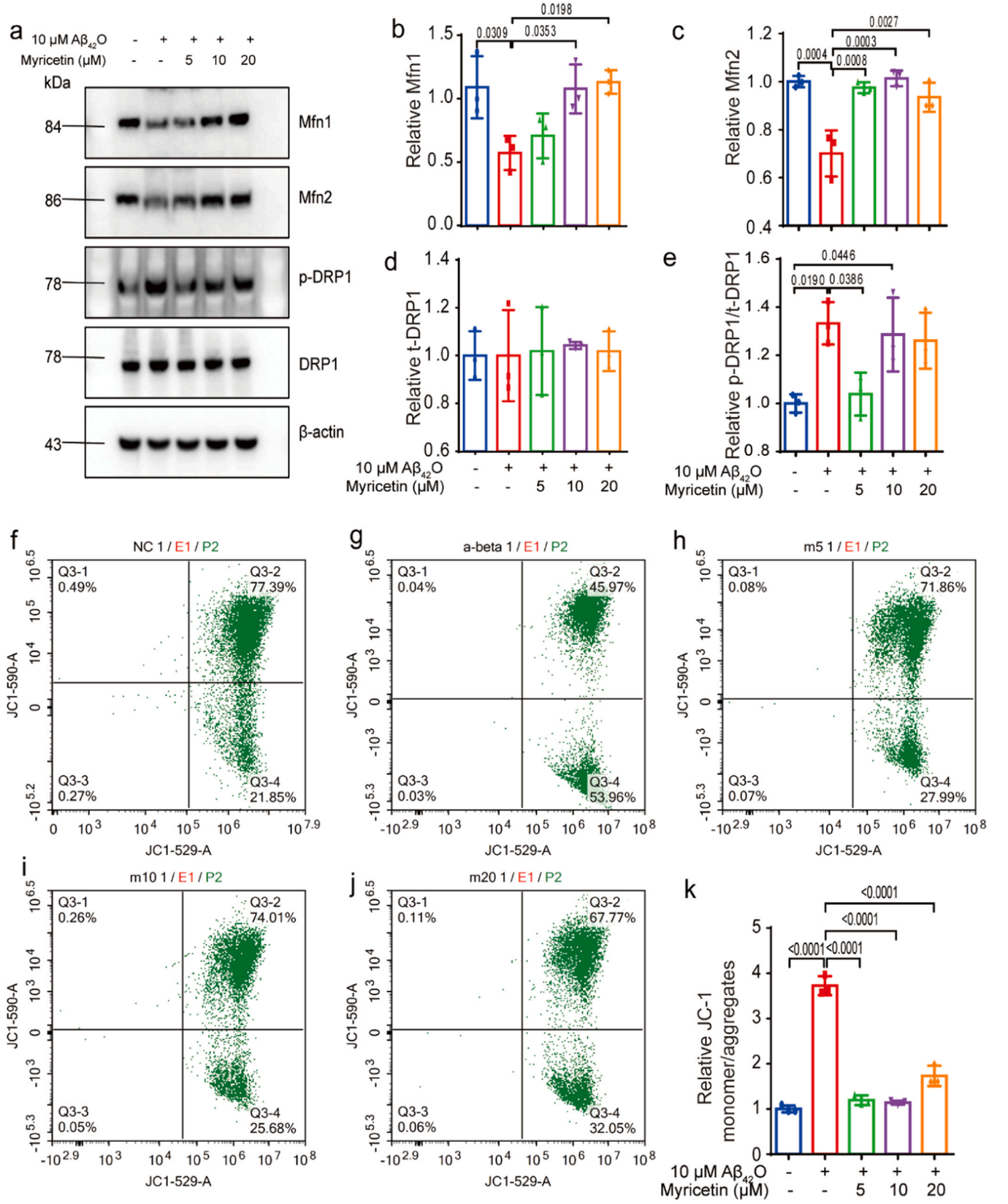

Fig. 7. Myricetin regulated the $A\beta_{42}O$-induced reduction in mitochondrial fusion proteins, phosphorylation of mitochondrial division proteins, and ΔΨm depolarization in SH-SY5Y cells. (**a-e**) Representative blots and quantification of mitochondrial fusion proteins (Mfn1 and Mfn2) and mitochondrial division (t-DRP1 and p-DRP1/t-DRP1) (n=3). The values were normalized to those of the control. (**f-k**) Analysis of the ΔΨm via JC-1 staining and flow cytometry (n=3). (f) Control, (g) 10 μM $A\beta_{42}O$ treatment, (h) 10 μM $A\beta_{42}O$ + 5 μM myricetin treatment, (d) 10 μM $A\beta_{42}O$ + 10 μM myricetin treatment, (d) 10 μM $A\beta_{42}O$ + 20 μM myricetin treatment, (d) Quantification of green/red fluorescence intensity (normalized to the control). One-way ANOVA and Tukey's multiple comparison test were used.

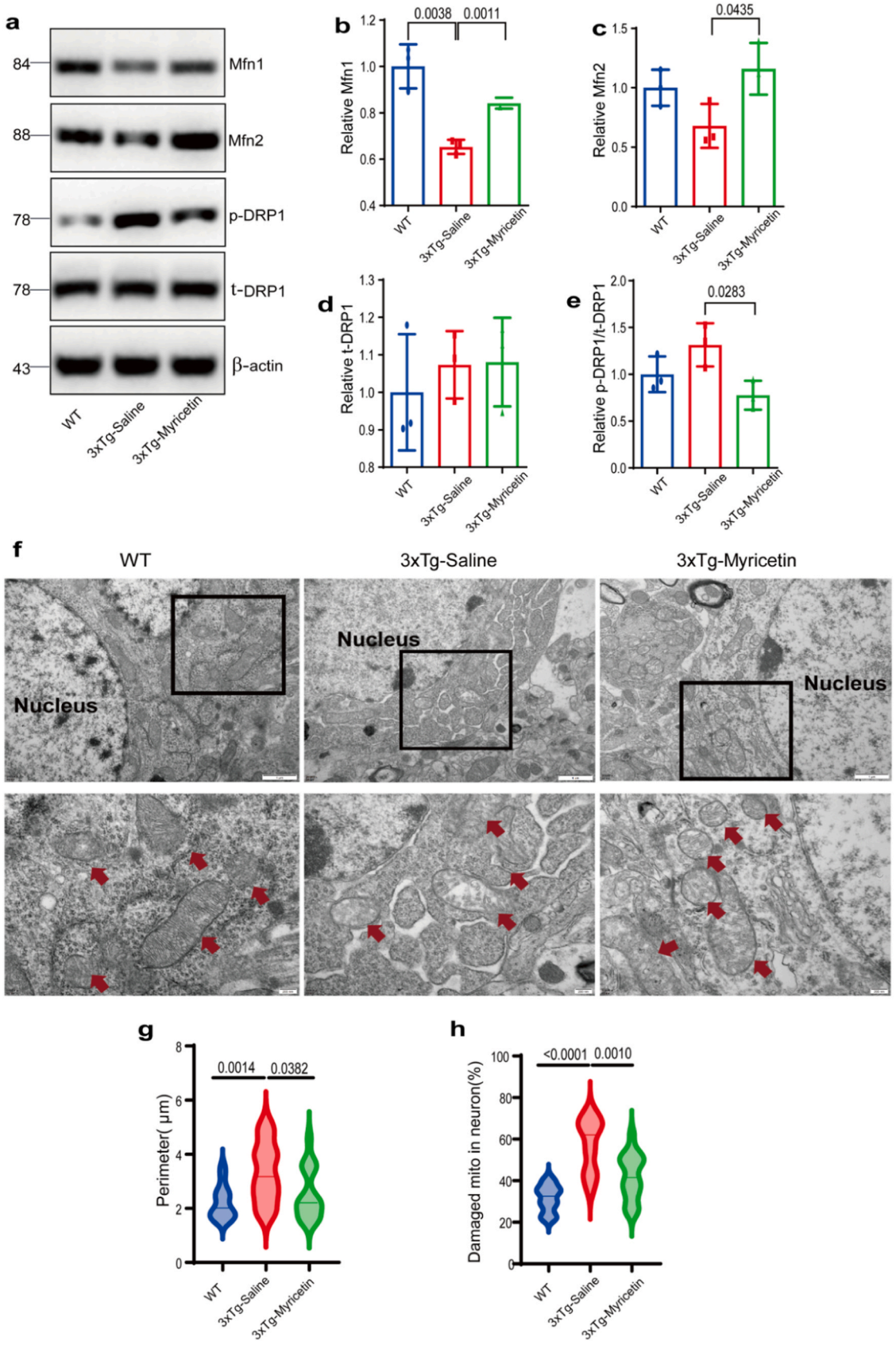

Fig. 8. Myricetin regulated the expression of mitochondrial fusion proteins, the phosphorylation of division proteins, and mitochondrial morphological changes in the hippocampi of 3×Tg mice. (**a-e**) Representative blots and quantification of mitochondrial fusion proteins (Mfn1 and Mfn2) and division proteins (t-DRP1 and p-DRP1/t-DRP1) (n=3). The values were normalized to those of the control. (**f**) Representative TEM images of mitochondrial structures in neurons from the hippocampi of the WT, 3×Tg-saline and 3×Tg-myricetin groups are shown, as indicated by the arrow. (**g, h**) Comparison of perimeter and damaged mito percent among the WT, 3×Tg-saline and 3×Tg-myricetin groups. One-way ANOVA and Tukey's multiple comparison test were used.

10, 20 μM myricetin+$A\beta_{42}O$ vs. $A\beta_{42}O$) (Fig. 7**f-k**).

3.8. Myricetin blocked ROS production, lipid peroxidation, and DNA oxidation in SH-SY5Y cells and in 3×Tg mice

Next, we evaluated the effects of myricetin on $A\beta_{42}O$-induced ROS generation in SH-SY5Y cells by using flow cytometry with a DCFH-DA assay. We found that treatment with $A\beta_{42}O$ (10 μM) increased ROS levels by 24 % (p=0.0037, control vs. $A\beta_{42}O$ group), which was completely blocked by myricetin (5 μM p=0.0137, 10 μM 0,0367, myricetin + $A\beta_{42}O$ vs. $A\beta_{42}O$ group) (Fig. 9a-f). We found that treatment with $A\beta_{42}O$ (10 μM) increased lipid peroxidation, as indicated by the increase in 8-OHdG fluorescence intensity, by 61 % (p<0.0001, control vs. $A\beta_{42}O$ group). treatment with myricetin (5. 10, 20 μM) prevented this $A\beta_{42}O$ (10 μM)-induced increase in 8-OHdG fluorescence intensity in SH-SY5Y cells (p<0.0001 for all groups, myricetin+ $A\beta_{42}O$ vs. $A\beta_{42}O$ group) (Fig. 9 g). Furthermore, we found that treatment with $A\beta_{42}O$ (10 μM) increased lipid peroxidation, as indicated by a 116 % increase in 4-HNE fluorescence intensity (p<0.0001, control vs. $A\beta_{42}O$ group). treatment with myricetin (5. 10, 20 μM) prevented this $A\beta_{42}O$ (10 μM)-induced increase in 4-HNE fluorescence intensity in SH-SY5Y cells (p<0.0001 for 5. 10, 20 μM myricetin+ $A\beta_{42}O$ vs. $A\beta_{42}O$ group)

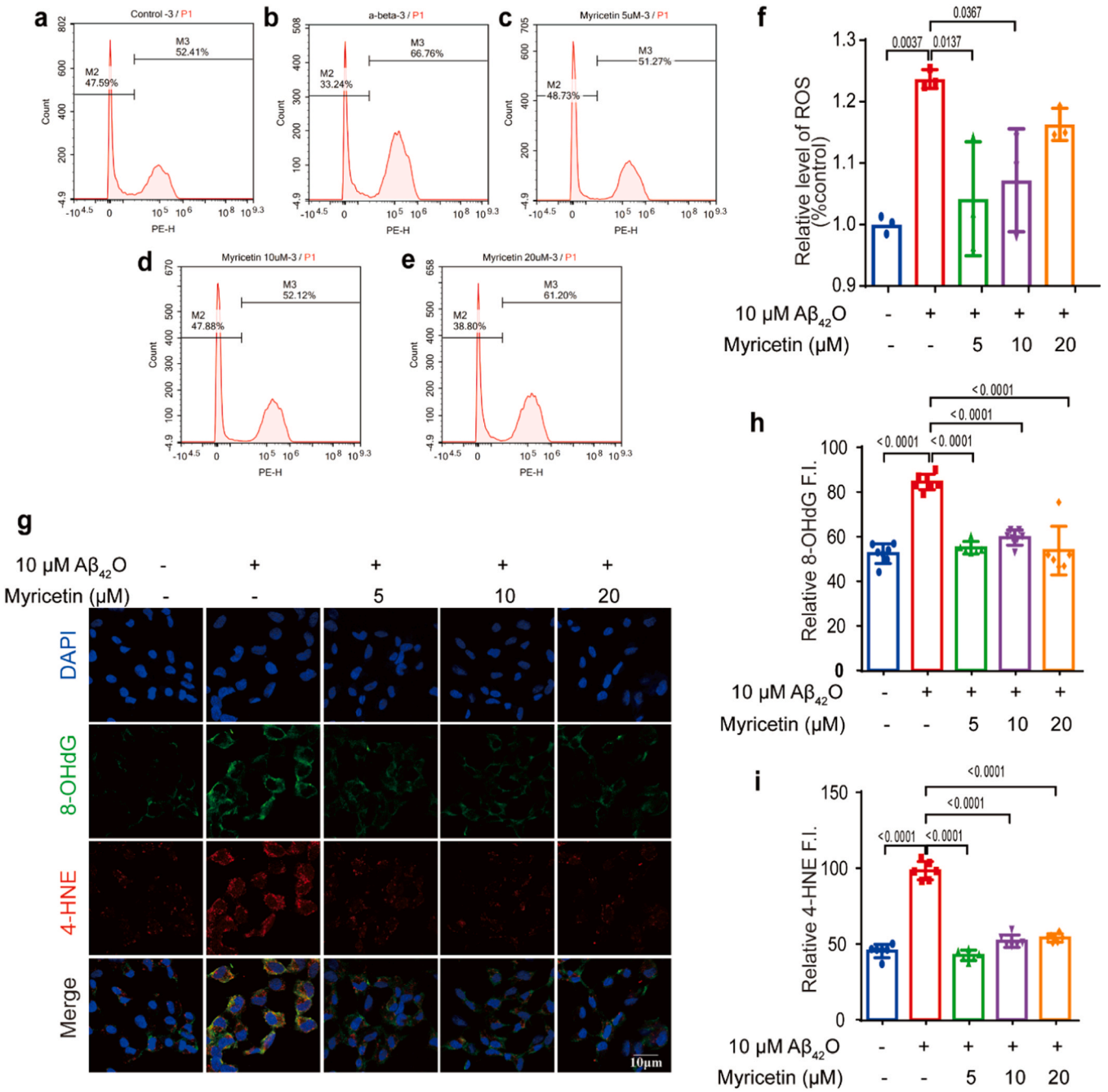

Fig. 9. Myricetin reversed the increase in lipid peroxidation and DNA oxidation in SH-SY5Y cells. (**a-f**) Flow cytometry analysis of ROS in combination with DCFH-DA. (a) Control, (b) 10 μM $A\beta_{42}O$ treatment, (c) 10 μM $A\beta_{42}O$+5 μM myricetin treatment, (d) 10 μM $A\beta_{42}O$+10 μM myricetin treatment, (d) 10 μM $A\beta_{42}O$+20 μM myricetin treatment, and (f) quantification of ROS (normalized to the control). (**g-i**) Representative confocal images and quantification of the immunoreactivity of (**g, h**) 8-OHdG. (**g, i**) 4-HNE. Nuclei were counterstained with DAPI; scale bar=10 μm (g). One hundred cells from each group were analysed. One-way ANOVA, Tukey's multiple comparison test.

(Fig. 9 h, i).

To determine the impact of myricetin on oxidative stress damage in 3×Tg mice in vivo, we measured the levels of 8-OHdG and 4-HNE in hippocampal brain tissue by using immunofluorescence assays. Compared with saline treatment, myricetin treatment (5. 10, 20 μM) reduced the 8-OHdG and 4-HNE fluorescence intensities in the cornu ammonis (CA) 1, dentate gyrus (DG), and CA3 regions of 3×Tg mice (8-OHdG: 5 μM p=0.0005, 10 μM p<0.0001, 20 μM p<0.0001; 4-HNE: 5 μM p<0.0001, 10 μM p<0.0001, 20 μM p=0.0029) (Fig. 10a-h).

4. Discussion

Here, we integrated the network pharmacology results of myricetin with the cell culture and in vivo treatment studies. We discovered strong interactions between myricetin and selected core targets, including APP, ERK2 (MAPK1), and GSK3β. Next, we demonstrated the ability of myricetin treatment to ameliorate cognitive impairment in 3×Tg mice. Myricetin treatment alleviated tau hyperphosphorylation, synaptic and mitochondrial impairment, ROS production and oxidation in both $A\beta_{42}O$-treated SH-SY5Y cells and 3×Tg mice through the inhibition of the hyperphosphorylation of the GSK3β and ERK2 signalling pathways.

We found that myricetin treatment (20 mg/kg, i.p., 14 days) improved the spatial cognition, learning and memory of 3×Tg mice, which is consistent with previous reports [29,53]. The dosage (20 mg/kg) and duration (14 days) of myricetin treatment used in the present study were within the ranges of earlier studies [29,53]. Decreased synaptic protein expression, indicative of impaired synaptic function [18–20,54], and increased levels of tau phosphorylation [21, 55] have been reported in cultured $A\beta_{42}O$-treated neurons and in 3×Tg mice. Myricetin has been previously shown to prevent Aβ oligomerization and neurofibrillary tangle formation and reduce neuronal plasticity (long-term potentiation and long-term depression) through site-specific binding to Aβ [39,56,57]. We also observed that myricetin 5 μM could alleviate the increase in the expression of APP induced by Aβ oligomers in SH-SY5Y cells. Concurrently, we found that myricetin treatment at 5, 10 μM in $A\beta_{42}O$-treated SH-SY5Y cells and at 20 mg/kg (i.p. daily. for 2 weeks) in 3×Tg mice restored synaptic impairment by decreasing the expression of presynaptic proteins (SNAP25 and synaptophysin) and postsynaptic protein PSD95 and the phosphorylation of tau, which has not been demonstrated previously.

We observed that myricetin reversed the reductions in the mitochondrial membrane potential, the expression of mitochondrial fusion

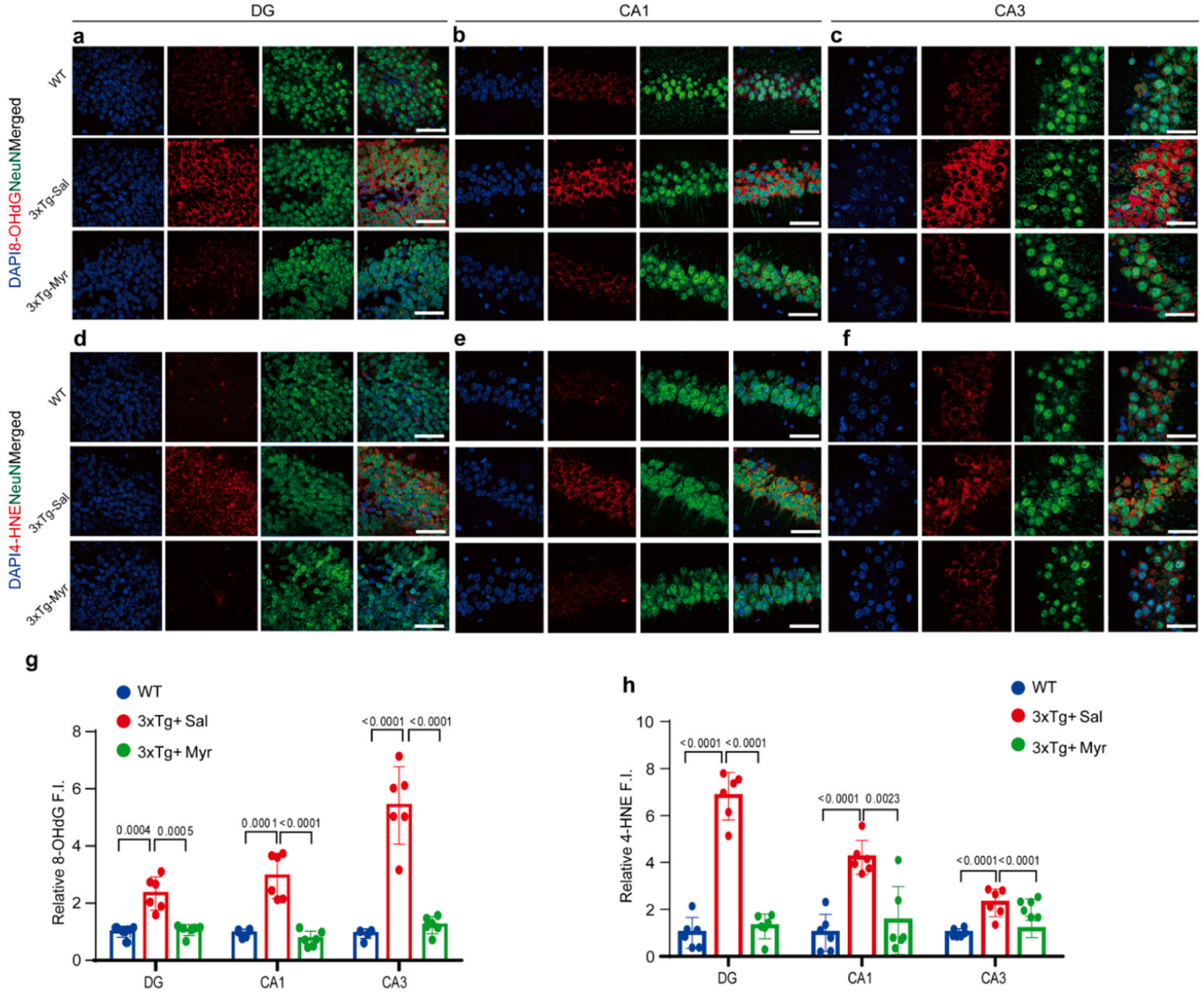

Fig. 10. Myricetin reversed ROS production, lipid peroxidation and DNA oxidation in 3×Tg mice. Representative confocal images and quantification of the immunoreactivity of (**a-c, g**) 8-OHdG and (**d-f, h**) 4-HNE and neurons in the dentate gyrus (DG)/corno ammon (CA)1/(CA)3 subfields of the hippocampus (n = 3). Nuclei were counterstained with DAPI (blue). Scale bar = 10 μm. One-way ANOVA, Tukey's multiple comparison test. Sal: saline; Myricetin, Myr.

proteins (Mfn1 at 10, 20 μM and Mfn2 at 5, 10, 20 μM), and the phosphorylation of mitochondrial fission protein (p-DRP1, at 5, 10 μM) in $A\beta_{42}O$-treated SH-SY5Y cells and 3×Tg mice (20 mg/kg, i.p., 14 days). Several studies have shown that Aβ and tau accumulation reduce the expression of Mfn1, Mfn2 and DRP1 in animal models of AD [13,58,59]. Our results are consistent with recent studies showing that myricetin prevents high-molecular-weight $A\beta_{42}$ oligomer-induced neurotoxicity through antioxidant effects on the cell membranes and mitochondria of HT-22 cells [38] and by restoring Aβ-induced mitochondrial impairments in N2a-SW cells [35]. However, Aβ may not be the only disease-causing protein involved in the course of AD. Intraneuronal tangles containing hyperphosphorylated tau are a hallmark of AD pathology[60], and tau is a mediator of Aβ cytotoxicity[61]. However, our findings contrast with those of a previous report showing the stable expression of various fission/fusion-mediating proteins, such as Mfn1 and Mfn2, and the phosphorylation of DRP1 after 1–6 h of Aβ treatment [62]. The potential reason for this difference is the duration of treatment with Aβ and the forms of Aβ oligomers used in different studies. A recent study indicated the involvement of mitochondrial fission and mitophagy in Aβ oligomer-induced synaptotoxicity [63]. Phosphorylation of DRP1 has been reported to activate DRP1-mediated fission, and translocation of DRP1 is important for the initiation of fission [64]. In our study, we also detected a positive effect of myricetin extract on mitochondrial morphology in hippocampal tissue via electron microscopy.

We found that myricetin prevented the increased generation of intracellular ROS (at 10, 20 μM), lipid peroxidation (4-HNE, at 5, 10, 20 μM), and DNA oxidation (8-OHdG, at 5, 10, 20 μM) in $A\beta_{42}O$-treated SH-SY5Y cells. A similar effect was observed in the treatment with myricetin in 3×Tg mice (at 20 mg/kg, i.p., daily, 2 weeks). These findings are consistent with previous reports that myricetin reduces lipid peroxidation and DNA oxidation in human periodontal ligament stem cells [65]. ROS overproduction is known to interfere with the equilibrium between oxidants and antioxidant capacity, leading to extensive damage to subcellular structures, mitochondrial dysfunction, lipid peroxidation, and DNA damage [5,66]. The reciprocal association between mitochondrial fusion proteins and ROS in Aβ-treated neurons has been reported previously [62,67].

Moreover, we found that myricetin showed reduction against $A\beta_{42}O$ induced phosphorylation of ERK2 (MAPK1) (at 5, 10 μM) and GSK3β (at 5, 10, 20 μM) in SH-SY5Y cells. The two pathways w were also involved in the protective effect of myricetin treatment (20 mg/kg, i.p., 2 weeks) in 3×Tg mice. This observation is in line with previous findings on the effect of myricetin on the ERK2 (MAPK1) and GSK3β pathways [51,68]. ERK2 (MAPK1) plays a central role in oxidative stress in AD, is involved in tau phosphorylation [69,70] and is a potential therapeutic target in various neurodegenerative disorders [71]. GSK3β, a downstream protein kinase of AKT, plays an important role in tau hyperphosphorylation, the regulation of hippocampal neurogenesis and synaptic plasticity and is involved in mitochondrial function [72–74]. Here we found that p-GSK3β Ser9, an inactive form of GSK3β was increased, while p-GSK3β Tyr216 (the active form) was increased in 3×Tg-myricetin mice compared to 3×Tg-saline mice. These alteration in p-GSK3β contributed to the reduction in the downstream tau phosphorylation in 3×Tg-myricetin mice compared to 3×Tg-saline mice [75,76].

Aggregated Aβ induces tau hyperphosphorylation by enhancing the activity of GSK3β [77]. GSK3β also functions in DNA repair by phosphorylating DNA repair factors and influencing their binding to chromatin [73]. To clarify the relationship between ERK2 (MAPK1) and GSK3β in this study, we included inhibitors of these two signaling pathway proteins in the experiment. Surprisingly, we found that these two inhibitors not only inhibit their respective signaling pathways, but also inhibit other signaling pathways simultaneously. Therefore, we hypothesize that ERK2 (MAPK1) and GSK3β signaling pathways show synergistic effects on myricetin improvement of AD pathology, suggesting that there may be cross-action or mutual promotion between the two pathways. Whether there is interaction between the two target proteins still needs further study and discussion. Myricetin may inhibit the phosphorylation of ERK1/2 and GSK3β primarily through indirect mechanisms rather than direct binding: Myricetin has potent antioxidant properties, which can reduce the levels of ROS within cells, which is known to activate ERK1/2 signaling pathways. By reducing oxidative stress, myricetin can indirectly inhibit the activation (phosphorylation) of ERK1/2 [78,79]. Moreover, myricetin may affect upstream kinases that are responsible for the activation of ERK1/2, such as inhibiting the activity of MEK (MAPK/ERK kinase), which directly phosphorylates and activates ERK1/2 [80]. GSK3β is regulated by the PI3K/Akt signaling pathway, where Akt phosphorylates and inhibits GSK3β. Myricetin can activate the PI3K/Akt pathway, leading to the phosphorylation (and thus inhibition) of GSK3β. This indirect mechanism involves enhancing Akt activity rather than binding directly to GSK3β [81]. Myricetin can block BTK/ERK and BTK/AKT signal transduction cascades (including downstream substrates GSK3β, IKK, STAT3, and NF-κB) [82]. While direct binding to GSK3β has been proposed in some studies, the primary mechanism seems to involve modulation of upstream kinases and pathways that regulate GSK3β. Some research suggests that flavonoids, including myricetin, can bind to ATP-binding sites of kinases, potentially leading to direct inhibition. However, the predominant evidence supports an indirect regulatory mechanism.

The differential effect of myricetin at varying concentrations (5, 10, and 20 μM) on cellular outcomes can be attributed to several factors, including: 1) Concentration-dependent efficacy: Many bioactive compounds exhibit a bell-shaped dose-response curve where there is an optimal concentration (middle level of concentration) that provides the maximum therapeutic benefit. For myricetin, 5 μM might be the optimal concentration for reducing p-TauS396, ROS, p-DRP1, pGSK3β, and increasing synaptic protein levels. At higher concentrations (10 or 20 μM), the compound may lose its efficacy due to various factors such as receptor saturation or negative feedback mechanisms. 2) Cellular Toxicity: Higher concentrations of myricetin (10 or 20 μM) could lead to cytotoxic effects, resulting in cellular stress or damage that offsets its therapeutic benefits. This can manifest as increased ROS production or other forms of cellular stress that negate the positive effects observed at lower concentrations. While myricetin has antioxidant properties at lower concentrations, at higher concentrations, it might paradoxically act as a pro-oxidant, increasing ROS levels and causing oxidative damage to cellular components, including proteins, lipids, and DNA. 3) Pathway and enzyme interaction: At lower concentrations, myricetin might inhibit enzymes like GSK3β and DRP1 effectively, thereby reducing p-TauS396 and p-DRP1 levels. However, at higher concentrations, it might inhibit these enzymes too much or non-specifically, leading to dysregulation of normal cellular functions. Myricetin's interaction with various signaling pathways might be concentration-dependent. At 5 μM, it might enhance beneficial pathways (e.g., antioxidant defenses, synaptic protein expression) and suppress harmful ones (e.g., tau phosphorylation, ROS generation). At higher concentrations, these pathways might become overstimulated or inhibited excessively, leading to suboptimal or adverse outcomes. 4) Pharmacokinetics and Bioavailability: The cellular uptake of myricetin could be optimized at 5 μM, ensuring adequate intracellular concentrations for therapeutic effects. At higher concentrations, the compound might saturate the transport mechanisms or undergo rapid metabolism and degradation, reducing its effective intracellular concentration and activity.

Here we have assessed only three tau phosphoepitopes p-TauS396, p-TauT231 and p-TauS356 in the brain tissue from 3×Tg mice, and observed consistent alterations in these three phosphoepitopes. Alteration in the phosphorylation of tau at TauT231 or TauS396 plays a crucial role in hyperphosphorylation and formation of tau tangle in AD brains, and that phosphorylation of tau at sites Ser396–404 is one of the early events in AD [83–85]. Given the complexity in tau phosphorylation processes, analysis of other phosphorylation sites of tau by using Western blotting as well as immunofluorescence staining would be

useful in the further study.

There are several limitations in our study. 1) In the in vitro experiment, we observed that at a higher concentration (20 μM), myricetin reduced cell viability, which is quite close to the effective dosage of 5 μM. 2) In vivo treatment study in 3×Tg mice is a single dosing design and with only Morris Water Maze test being used as the outcome measure for the cognitive improvement. Further studies using different escalating doses of myricetin for treatment and additional behavioural test panels will be critical. 4) The mechanistic study had a limited scope. Moreover we focused on the pathway related to Tau protein phosphorylation and the involvement of only GSK3β and the ERK2 (MAPK1) pathway. Other pathways including the effect on amyloid-genic pathway, and ERK/JNK/p38 mitogen-activated protein kinase signalling pathways, the mTOR pathway, and the ATG5-dependent autophagy pathway, have also been implicated in the effect of myricetin [26,65].

5. Conclusions

We showed that myricetin treatment ameliorated cognitive impairment in 3×Tg mice and reduced tau hyperphosphorylation, impairment of pre- and postsynaptic proteins, mitochondrial function, ROS generation, lipid peroxidation, and DNA oxidation in both cell culture and in a 3×Tg mouse model. Furthermore, hyperphosphorylation of the GSK3β and ERK2 (MAPK1) signalling pathways was involved in the protective effect of myricetin treatment. These findings provide new insights into the protective mechanism of myricetin as a potential treatment for AD.

Ethics approval and consent to participate

All animal experiments were approved by the Institutional Animal Care and Use Committee of Guizhou Medical University (approval No. 2304543). All the experiments were complied with the ARRIVE 2.0 guidelines and were performed in accordance with guidelines under the approval of the Animal Protection and Use Committee of Guizhou Medical University.

Consent for publication

Not applicable.

Funding

This work was supported by the Chinese National Natural Science Foundation (82260263), the Guizhou Provincial Science and Technology Program Project Grant (Qiankehe Platform Talents-GCC[2023] 035), the Guizhou Science and Technology Plan Project (Guizhou Science Support [2023] General 232), the Guizhou Provincial Science and Technology Program Project Grant (ZK[2024]042), the Guizhou Association for Science and Technology (project number GZYZ2023-04), the National Natural Science Foundation (NSFC) Youth Fund Cultivation Program of the Affiliated Hospital of Guizhou Medical University (gyfynsfc-2022053), Guizhou Provincial Department of Education Youth Science and Technology Talent Project (QianJiaoji [2024]92), and the Science and Technology Fund Project of the Guizhou Provincial Health Commission (WT22007).

CRediT authorship contribution statement

Zhi Tang: Writing – review & editing, Supervision, Resources, Project administration, Conceptualization. **Li Wang:** Writing – original draft, Formal analysis, Data curation, Conceptualization. **Xiaolan Qi:** Writing – review & editing, Supervision, Resources, Funding acquisition, Conceptualization. **Ruiqing Ni:** Writing – review & editing, Supervision, Conceptualization. **Yan Xiao:** Writing – review & editing, Formal analysis, Data curation. **Xi Yang:** Writing – review & editing, Formal analysis, Data curation. **Yaqian Peng:** Writing – review & editing, Formal analysis, Data curation. **Bo Li:** Writing – review & editing, Formal analysis, Data curation.

Declaration of Competing Interest

The authors declare that they have no known competing financial interests or personal relationships that could have appeared to influence the work reported in this paper.

Data Availability

Data will be made available on request.

Appendix A. Supporting information

Supplementary data associated with this article can be found in the online version at doi:10.1016/j.biopha.2024.116963.

References

[1] 2022 Alzheimer's disease facts and figures, Alzheimer's & dementia: the journal of the Alzheimer's Association 18(4) (2022) 700–789..
[2] D.S. Knopman, H. Amieva, R.C. Petersen, G. Chételat, D.M. Holtzman, B.T. Hyman, R.A. Nixon, D.T. Jones, Alzheimer disease, Nat. Rev. Dis. Prim. 7 (1) (2021) 33.
[3] J. Wang, Q. Huang, K. He, J. Li, T. Guo, Y. Yang, Z. Lin, S. Li, G. Vanderlinden, Y. Huang, K. Van Laere, Y. Guan, Q. Guo, R. Ni, B. Li, F. Xie, Presynaptic density determined by SV2A PET is closely associated with postsynaptic metabotropic glutamate receptor 5 availability and independent of amyloid pathology in early cognitive impairment, Alzheimers Dement (2024).
[4] M. Tzioras, R.I. McGeachan, C.S. Durrant, T.L. Spires-Jones, Synaptic degeneration in Alzheimer disease, Nat. Rev. Neurol. 19 (1) (2023) 19–38.
[5] M.W. Park, H.W. Cha, J. Kim, J.H. Kim, H. Yang, S. Yoon, N. Boonpraman, S.S. Yi, I.D. Yoo, J.S. Moon, NOX4 promotes ferroptosis of astrocytes by oxidative stress-induced lipid peroxidation via the impairment of mitochondrial metabolism in Alzheimer's diseases, Redox Biol. 41 (2021) 101947.
[6] Z. Tang, Z. Chen, M. Guo, Y. Peng, Y. Xiao, Z. Guan, R. Ni, X. Qi, NRF2 deficiency promotes ferroptosis of astrocytes mediated by oxidative stress in Alzheimer's disease, Mol. Neurobiol. (2024).
[7] J. Zhang, L. Liu, Y. Zhang, Y. Yuan, Z. Miao, K. Lu, X. Zhang, R. Ni, H. Zhang, Y. Zhao, X. Wang, ChemR23 signaling ameliorates cognitive impairments in diabetic mice via dampening oxidative stress and NLRP3 inflammasome activation, Redox, Biology 58 (2022) 102554.
[8] D.A. Butterfield, B. Halliwell, Oxidative stress, dysfunctional glucose metabolism and Alzheimer disease, Nat. Rev. Neurosci. 20 (3) (2019) 148–160.
[9] E.L. Feldman, B.C. Callaghan, R. Pop-Busui, D.W. Zochodne, D.E. Wright, D. L. Bennett, V. Bril, J.W. Russell, V. Viswanathan, Diabetic neuropathy, Nat. Rev. Dis. Prim. 5 (1) (2019) 41.
[10] S.M. Alavi Naini, N. Soussi-Yanicostas, Tau hyperphosphorylation and oxidative stress, a critical vicious circle in neurodegenerative tauopathies? Oxid. Med Cell Longev. 2015 (2015) 151979.
[11] T. Petrozziello, E.A. Bordt, A.N. Mills, S.E. Kim, E. Sapp, B.A. Devlin, A.A. Obeng-Marnu, S.M.K. Farhan, A.C. Amaral, S. Dujardin, P.M. Dooley, C. Henstridge, D. H. Oakley, A. Neueder, B.T. Hyman, T.L. Spires-Jones, S.D. Bilbo, K. Vakili, M. E. Cudkowicz, J.D. Berry, M. DiFiglia, M.C. Silva, S.J. Haggarty, G. Sadri-Vakili, Targeting tau mitigates mitochondrial fragmentation and oxidative stress in amyotrophic lateral sclerosis, Mol. Neurobiol. 59 (1) (2022) 683–702.
[12] M. Denechaud, S. Geurs, T. Comptdaer, S. Bégard, A. Garcia-Núñez, L. A. Pechereau, T. Bouillet, Y. Vermeiren, P.P. De Deyn, R. Perbet, V. Deramecourt, C.A. Maurage, M. Vanderhaegen, S. Vanuytven, B. Lefebvre, E. Bogaert, N. Déglon, T. Voet, M. Colin, L. Buée, B. Dermaut, M.C. Galas, Tau promotes oxidative stress-associated cycling neurons in S phase as a pro-survival mechanism: Possible implication for Alzheimer's disease, Prog. Neurobiol. (2022) 102386.
[13] R. Kandimalla, M. Manczak, X. Yin, R. Wang, P.H. Reddy, Hippocampal phosphorylated tau induced cognitive decline, dendritic spine loss and mitochondrial abnormalities in a mouse model of Alzheimer's disease, Hum. Mol. Genet. 27 (1) (2018) 30–40.
[14] M. Xu, H. Huang, X. Mo, Y. Zhu, X. Chen, X. Li, X. Peng, Z. Xu, L. Chen, S. Rong, W. Yang, S. Liu, L. Liu, Quercetin-3-O-Glucuronide Alleviates Cognitive Deficit and Toxicity in Aβ(1-42) -Induced AD-Like Mice and SH-SY5Y, Cells, Mol. Nutr. Food Res. 65 (6) (2021) e2000660.
[15] G.H. Zhang, R.B. Pare, K.L. Chin, Y.H. Qian, Tβ4 ameliorates oxidative damage and apoptosis through ERK/MAPK and 5-HT1A signaling pathway in Aβ insulted SH-SY5Y cells, Life Sci. (2021) 120178.
[16] E. Lauretti, O. Dincer, D. Praticò, Glycogen synthase kinase-3 signaling in Alzheimer's disease, Biochimica et biophysica acta, Mol. Cell Res. 1867 (5) (2020) 118664.
[17] M.R. Khezri, K. Yousefi, A. Esmaeili, M. Ghasemnejad-Berenji, The role of ERK1/2 pathway in the pathophysiology of Alzheimer's disease: an overview and update on new developments, Cell. Mol. Neurobiol. (2022).

[18] I. Benilova, E. Karran, B. De, Strooper, The toxic Aβ oligomer and Alzheimer's disease: an emperor in need of clothes, Nat. Neurosci. 15 (3) (2012) 349–357.
[19] G.M. Shankar, S. Li, T.H. Mehta, A. Garcia-Munoz, N.E. Shepardson, I. Smith, F. M. Brett, M.A. Farrell, M.J. Rowan, C.A. Lemere, C.M. Regan, D.M. Walsh, B. L. Sabatini, D.J. Selkoe, Amyloid-β protein dimers isolated directly from Alzheimer's brains impair synaptic plasticity and memory, Nat. Med. 14 (8) (2008) 837–842.
[20] G. Brinkmalm, W. Hong, Z. Wang, W. Liu, T.T. O'Malley, X. Sun, M.P. Frosch, D. J. Selkoe, E. Portelius, H. Zetterberg, K. Blennow, D.M. Walsh, Identification of neurotoxic cross-linked amyloid-β dimers in the Alzheimer's brain, Brain 142 (5) (2019) 1441–1457.
[21] M.A. Busche, B.T. Hyman, Synergy between amyloid-β and tau in Alzheimer's disease, Nat. Neurosci. 23 (10) (2020) 1183–1193.
[22] T.M. Holland, P. Agarwal, Y. Wang, S.E. Leurgans, D.A. Bennett, S.L. Booth, M. C. Morris, Dietary flavonols and risk of Alzheimer dementia, Neurology 94 (16) (2020) e1749-e1756.
[23] T.M. Holland, P. Agarwal, Y. Wang, K. Dhana, S.E. Leurgans, K. Shea, S.L. Booth, K. Rajan, J.A. Schneider, L.L. Barnes, Association of Dietary Intake of Flavonols With Changes in Global Cognition and Several Cognitive Abilities, Neurology (2022).
[24] Q. Wang, X. Dong, R. Zhang, C. Zhao, Flavonoids with potential anti-amyloidogenic effects as therapeutic drugs for treating Alzheimer's disease, J. Alzheimers Dis. 84 (2) (2021) 505–533.
[25] X. Song, L. Tan, M. Wang, C. Ren, C. Guo, B. Yang, Y. Ren, Z. Cao, Y. Li, J. Pei, Myricetin: A review of the most recent research, Biomedicine & pharmacotherapy = Biomedecine & pharmacotherapie 134 (2021) 111017.
[26] B. Dai, T. Zhong, Z.X. Chen, W. Chen, N. Zhang, X.L. Liu, L.Q. Wang, J. Chen, Y. Liang, Myricetin slows liquid-liquid phase separation of Tau and activates ATG5-dependent autophagy to suppress Tau toxicity, J. Biol. Chem. 297 (4) (2021) 101222.
[27] X. Pan, T. Chen, Z. Zhang, X. Chen, C. Chen, L. Chen, X. Wang, X. Ying, Activation of Nrf2/HO-1 signal with Myricetin for attenuating ECM degradation in human chondrocytes and ameliorating the murine osteoarthritis, Int. Immunopharmacol. 75 (2019) 105742.
[28] W.L. Sun, X.Y. Li, H.Y. Dou, X.D. Wang, J.D. Li, L. Shen, H.F. Ji, Myricetin supplementation decreases hepatic lipid synthesis and inflammation by modulating gut microbiota, Cell Rep. 36 (9) (2021) 109641.
[29] M. Ramezani, N. Darbandi, F. Khodagholi, A. Hashemi, Myricetin protects hippocampal CA3 pyramidal neurons and improves learning and memory impairments in rats with Alzheimer's disease, Neural Regen. Res. 11 (12) (2016) 1976–1980.
[30] Y. Taheri, H.A.R. Suleria, N. Martins, O. Sytar, A. Beyatli, B. Yeskaliyeva, G. Seitimova, B. Salehi, P. Semwal, S. Painuli, A. Kumar, E. Azzini, M. Martorell, W. N. Setzer, A. Maroyi, J. Sharifi-Rad, Myricetin bioactive effects: moving from preclinical evidence to potential clinical applications, BMC Complement Med Ther. 20 (1) (2020) 241.
[31] T. Hamaguchi, K. Ono, A. Murase, M. Yamada, Phenolic compounds prevent Alzheimer's pathology through different effects on the amyloid-beta aggregation pathway, Am. J. Pathol. 175 (6) (2009) 2557–2565.
[32] Y. Shimmyo, T. Kihara, A. Akaike, T. Niidome, H. Sugimoto, Multifunction of myricetin on A beta: neuroprotection via a conformational change of A beta and reduction of A beta via the interference of secretases, J. Neurosci. Res. 86 (2) (2008) 368–377.
[33] S. Chakraborty, S. Kumar, S. Basu, Conformational transition in the substrate binding domain of β-secretase exploited by NMA and its implication in inhibitor recognition: BACE1-myricetin a case study, Neurochem. Int. 58 (8) (2011) 914–923.
[34] J. Feng, J.X. Wang, Y.H. Du, Y. Liu, W. Zhang, J.F. Chen, Y.J. Liu, M. Zheng, K. J. Wang, G.Q. He, Dihydromyricetin inhibits microglial activation and neuroinflammation by suppressing NLRP3 inflammasome activation in APP/PS1 transgenic mice, CNS Neurosci. Ther. 24 (12) (2018) 1207–1218.
[35] X. Yao, J. Zhang, Y. Lu, Y. Deng, R. Zhao, S. Xiao, Myricetin Restores Aβ-Induced Mitochondrial Impairments in N2a-SW Cells, ACS Chem. Neurosci. 13 (4) (2022) 454–463.
[36] V. Mendes, R. Vilaça, V. de Freitas, P.M. Ferreira, N. Mateus, V. Costa, Effect of myricetin, pyrogallol, and phloroglucinol on yeast resistance to oxidative stress, Oxid. Med. Cell. Longev. 2015 (2015) 782504.
[37] M.U. Rehman, I.A. Rather, Myricetin abrogates cisplatin-induced oxidative stress, inflammatory response, and goblet cell disintegration in colon of wistar rats, Plants 9 (1) (2019).
[38] A.M. Kimura, M. Tsuji, T. Yasumoto, Y. Mori, T. Oguchi, Y. Tsuji, M. Umino, A. Umino, T. Nishikawa, S. Nakamura, T. Inoue, Y. Kiuchi, M. Yamada, D. B. Teplow, K. Ono, Myricetin prevents high molecular weight Aβ(1-42) oligomer-induced neurotoxicity through antioxidant effects in cell membranes and mitochondria, Free Radic. Biol. Med 171 (2021) 232–244.
[39] R. Pluta, S. Januszewski, S.J. Czuczwar, Myricetin as a promising molecule for the treatment of post-ischemic brain neurodegeneration, Nutrients 13 (2) (2021).
[40] T. Halder, B. Patel, N. Acharya, Design and optimization of myricetin encapsulated nanostructured lipid carriers: In-vivo assessment against cognitive impairment in amyloid beta ((1-42)) intoxicated rats, Life Sci. 297 (2022) 120479.
[41] P. Qiao, F. Zhao, M. Liu, D. Gao, H. Zhang, Y. Yan, Hydrogen sulfide inhibits mitochondrial fission in neuroblastoma N2a cells through the Drp1/ERK1/2 signaling pathway, Mol. Med. Rep. 16 (1) (2017) 971–977.
[42] S. Dai, F. Zhou, J. Sun, Y. Li, NPD1 enhances autophagy and reduces hyperphosphorylated tau and amyloid-β42 by inhibiting GSK3β activation in N2a/APP695swe cells, J. Alzheimer'S. Dis.: JAD 84 (2) (2021) 869–881.
[43] Q. Chen, C. Lai, F. Chen, Y. Ding, Y. Zhou, S. Su, R. Ni, Z. Tang, Emodin protects SH-SY5Y cells against zinc-induced synaptic impairment and oxidative stress through the ERK1/2 pathway, Front. Pharmacol. 13 (2022) 821521.
[44] Z. Tang, C.C. Lai, J. Luo, Y.T. Ding, Q. Chen, Z.Z. Guan, Mangiferin prevents the impairment of mitochondrial dynamics and an increase in oxidative stress caused by excessive fluoride in SH-SY5Y cells, J. Biochem. Mol. Toxicol. 35 (4) (2021) e22705.
[45] S. Oddo, A. Caccamo, J.D. Shepherd, M.P. Murphy, T.E. Golde, R. Kayed, R. Metherate, M.P. Mattson, Y. Akbari, F.M. LaFerla, Triple-transgenic model of Alzheimer's disease with plaques and tangles: intracellular Abeta and synaptic dysfunction, Neuron 39 (3) (2003) 409–421.
[46] Y. Kong, C.A. Maschio, X. Shi, F. Xie, C. Zuo, U. Konietzko, K. Shi, A. Rominger, J. Xiao, Q. Huang, R.M. Nitsch, Y. Guan, R. Ni, Relationship between reactive astrocytes, by [(18)F]SMBT-1 Imaging, with amyloid-beta, tau, glucose metabolism, and TSPO in mouse models of Alzheimer's disease, Mol. Neurobiol. (2024).
[47] Y. Kong, L. Cao, J. Wang, J. Zhuang, Y. Liu, L. Bi, Y. Qiu, Y. Hou, Q. Huang, F. Xie, Y. Yang, K. Shi, A. Rominger, Y. Guan, H. Jin, R. Ni, Increased cerebral level of P2×7R in a tauopathy mouse model by PET using [(18)F]GSK1482160, ACS Chem. Neurosci. (2024).
[48] J. Ma, J. Liu, Y. Chen, H. Yu, L. Xiang, Myricetin improves impaired nerve functions in experimental diabetic rats, Front. Endocrinol. 13 (2022) 915603.
[49] C. Lai, Z. Chen, Y. Ding, Q. Chen, S. Su, H. Liu, R. Ni, Z. Tang, Rapamycin attenuated zinc-induced tau phosphorylation and oxidative stress in rats: involvement of dual mTOR/p70S6K and Nrf2/HO-1, Pathw., Front. Immunol. 13 (2022) 782434.
[50] Z. Tang, M. Guo, Y. Peng, T. Zhang, Y. Xiao, R. Ni, X. Qi, Quercetin reduces APP expression, oxidative stress and mitochondrial dysfunction in the N2a/APPswe cells via ERK1/2 and AKT pathways, bioRxiv (2022), 2022.09.18.508406.
[51] J. Li, H. Xiang, C. Huang, J. Lu, Pharmacological actions of myricetin in the nervous system: a comprehensive review of preclinical studies in animals and cell models, Front Pharm. 12 (2021) 797298.
[52] Z. Tang, Y. Peng, Y. Jiang, L. Wang, M. Guo, Z. Chen, C. Luo, T. Zhang, Y. Xiao, R. Ni, X. Qi, Gastrodin ameliorates synaptic impairment, mitochondrial dysfunction and oxidative stress in N2a/APP cells, Biochem Biophys. Res Commun. 719 (2024) 150127.
[53] P. Liu, Y. Zhou, J. Shi, F. Wang, X. Yang, X. Zheng, Y. Wang, Y. He, X. Xie, X. Pang, Myricetin improves pathological changes in 3×Tg-AD mice by regulating the mitochondria-NLRP3 inflammasome-microglia channel by targeting P38 MAPK signaling pathway, Phytomedicine: Int. J. Phytother. Phytopharm. 115 (2023) 154801.
[54] D. Puzzo, R. Piacentini, M. Fá, W. Gulisano, D.D. Li Puma, A. Staniszewski, H. Zhang, M.R. Tropea, S. Cocco, A. Palmeri, P. Fraser, L. D'Adamio, C. Grassi, O. Arancio, LTP and memory impairment caused by extracellular Aβ and Tau oligomers is APP-dependent, eLife 6 (2017).
[55] L.K. Hamilton, G. Moquin-Beaudry, C.L. Mangahas, F. Pratesi, M. Aubin, A. Aumont, S.E. Joppé, A. Légiot, A. Vachon, M. Plourde, C. Mounier, M. Tétreault, K.J.L. Fernandes, Stearoyl-CoA Desaturase inhibition reverses immune, synaptic and cognitive impairments in an Alzheimer's disease mouse model, Nat. Commun. 13 (1) (2022) 2061.
[56] K. Ono, L. Li, Y. Takamura, Y. Yoshiike, L. Zhu, F. Han, X. Mao, T. Ikeda, J.-i Takasaki, H. Nishijo, A. Takashima, D.B. Teplow, M.G. Zagorski, M. Yamada, Phenolic compounds prevent amyloid β-protein oligomerization and synaptic dysfunction by site-specific binding*, J. Biol. Chem. 287 (18) (2012) 14631–14643.
[57] D. Liu, D. Du, Mulberry fruit extract alleviates cognitive impairment by promoting the clearance of amyloid-β and inhibiting neuroinflammation in Alzheimer's disease mice, Neurochem. Res. 45 (9) (2020) 2009–2019.
[58] A. Alexiou, G. Soursou, S. Chatzichronis, E. Gasparatos, M.A. Kamal, N.S. Yarla, A. Perveen, G.E. Barreto, G.M. Ashraf, Role of GTPases in the Regulation of Mitochondrial Dynamics in Alzheimer's Disease and CNS-Related Disorders, Mol. Neurobiol. 56 (6) (2019) 4530–4538.
[59] M. Manczak, R. Kandimalla, X. Yin, P.H. Reddy, Hippocampal mutant APP and amyloid beta-induced cognitive decline, dendritic spine loss, defective autophagy, mitophagy and mitochondrial abnormalities in a mouse model of Alzheimer's disease, Hum. Mol. Genet. 27 (8) (2018) 1332–1342.
[60] K.S. Kosik, C.L. Joachim, D.J. Selkoe, Microtubule-associated protein tau (tau) is a major antigenic component of paired helical filaments in Alzheimer disease, Proc. Natl. Acad. Sci. USA 83 (11) (1986) 4044–4048.
[61] S.A. Small, K. Duff, Linking Abeta and tau in late-onset Alzheimer's disease: a dual pathway hypothesis, Neuron 60 (4) (2008) 534–542.
[62] C.H. Hung, S.S. Cheng, Y.T. Cheung, S. Wuwongse, N.Q. Zhang, Y.S. Ho, S.M. Lee, R.C. Chang, A reciprocal relationship between reactive oxygen species and mitochondrial dynamics in neurodegeneration, Redox Biol. 14 (2018) 7–19.
[63] A. Lee, C. Kondapalli, D.M. Virga, T.L. Lewis Jr., S.Y. Koo, A. Ashok, G. Mairet-Coello, S. Herzig, M. Foretz, B. Viollet, R. Shaw, A. Sproul, F. Polleux, Aβ42 oligomers trigger synaptic loss through CAMKK2-AMPK-dependent effectors coordinating mitochondrial fission and mitophagy, Nat. Commun. 13 (1) (2022) 4444.
[64] N. Taguchi, N. Ishihara, A. Jofuku, T. Oka, K. Mihara, Mitotic phosphorylation of dynamin-related GTPase Drp1 participates in mitochondrial fission, J. Biol. Chem. 282 (15) (2007) 11521–11529.
[65] H.Y. Kim, S.Y. Park, S.Y. Choung, Enhancing effects of myricetin on the osteogenic differentiation of human periodontal ligament stem cells via BMP-2/Smad and ERK/JNK/p38 mitogen-activated protein kinase signaling pathway, Eur. J. Pharmacol. 834 (2018) 84–91.

[66] M. Zhao, Y. Wang, L. Li, S. Liu, C. Wang, Y. Yuan, G. Yang, Y. Chen, J. Cheng, Y. Lu, J. Liu, Mitochondrial ROS promote mitochondrial dysfunction and inflammation in ischemic acute kidney injury by disrupting TFAM-mediated mtDNA maintenance, Theranostics 11 (4) (2021) 1845–1863.
[67] S. Jiang, P. Nandy, W. Wang, X. Ma, J. Hsia, C. Wang, Z. Wang, M. Niu, S. L. Siedlak, S. Torres, H. Fujioka, Y. Xu, H.G. Lee, G. Perry, J. Liu, X. Zhu, Mfn2 ablation causes an oxidative stress response and eventual neuronal death in the hippocampus and cortex, Mol. Neurodegener. 13 (1) (2018) 5.
[68] Y. Jung, S.Y. Shin, Y.H. Lee, Y. Lim, Flavones with inhibitory effects on glycogen synthase kinase 3β, Appl. Biol. Chem. 60 (3) (2017) 227–232.
[69] S. Nagaraj, A. Want, K. Laskowska-Kaszub, A. Fesiuk, S. Vaz, E. Logarinho, U. Wojda, Candidate Alzheimer's disease biomarker miR-483-5p lowers TAU phosphorylation by Direct ERK1/2 repression, Int. J. Mol. Sci. 22 (7) (2021).
[70] M. Mai, X. Guo, Y. Huang, W. Zhang, Y. Xu, Y. Zhang, X. Bai, J. Wu, H. Zu, DHCR24 knockdown induces tau hyperphosphorylation at Thr181, Ser199, Ser262, and Ser396 sites via activation of the lipid raft-dependent Ras/MEK/ERK signaling pathway in C8D1A astrocytes, Mol. Neurobiol. 59 (9) (2022) 5856–5873.
[71] J.D. Iroegbu, O.K. Ijomone, O.M. Femi-Akinlosotu, O.M. Ijomone, ERK/MAPK signalling in the developing brain: Perturbations and consequences, Neurosci. Biobehav. Rev. 131 (2021) 792–805.
[72] B.M. Foidl, C. Humpel, Differential hyperphosphorylation of tau-S199, -T231 and -S396 in organotypic brain slices of Alzheimer Mice. A model to study early tau hyperphosphorylation using okadaic acid, Front. Aging Neurosci. 10 (2018) 113.
[73] W. Yang, Y. Liu, Q.Q. Xu, Y.F. Xian, Z.X. Lin, Sulforaphene ameliorates neuroinflammation and hyperphosphorylated tau protein via regulating the PI3K/Akt/GSK-3β pathway in experimental models of Alzheimer's disease, Oxid. Med. Cell. Longev. 2020 (2020) 4754195.
[74] K. Leroy, Z. Yilmaz, J.P. Brion, Increased level of active GSK-3beta in Alzheimer's disease and accumulation in argyrophilic grains and in neurones at different stages of neurofibrillary degeneration, Neuropathol. Appl. Neurobiol. 33 (1) (2007) 43–55.
[75] A. Takashima, GSK-3 is essential in the pathogenesis of Alzheimer's disease, J. Alzheimers Dis. 9 (3 Suppl) (2006) 309–317.
[76] F. Hernandez, J.J. Lucas, J. Avila, GSK3 and tau: two convergence points in Alzheimer's disease, J. Alzheimers Dis. 33 (Suppl 1) (2013). S141-4.
[77] H. Zempel, E. Thies, E. Mandelkow, E.M. Mandelkow, Abeta oligomers cause localized Ca(2+) elevation, missorting of endogenous Tau into dendrites, Tau phosphorylation, and destruction of microtubules and spines, J. Neurosci.: Off. J. Soc. Neurosci. 30 (36) (2010) 11938–11950.
[78] R. Zhong, L. Miao, H. Zhang, L. Tan, Y. Zhao, Y. Tu, M. Angel Prieto, J. Simal-Gandara, L. Chen, C. He, H. Cao, Anti-inflammatory activity of flavonols via inhibiting MAPK and NF-κB signaling pathways in RAW264.7 macrophages, Curr. Res Food Sci. 5 (2022) 1176–1184.
[79] W.T. Chiu, S.C. Shen, J.M. Chow, C.W. Lin, L.T. Shia, Y.C. Chen, Contribution of reactive oxygen species to migration/invasion of human glioblastoma cells U87 via ERK-dependent COX-2/PGE(2) activation, Neurobiol. Dis. 37 (1) (2010) 118–129.
[80] J.E. Kim, J.Y. Kwon, D.E. Lee, N.J. Kang, Y.S. Heo, K.W. Lee, H.J. Lee, MKK4 is a novel target for the inhibition of tumor necrosis factor-alpha-induced vascular endothelial growth factor expression by myricetin, Biochem Pharm. 77 (3) (2009) 412–421.
[81] Y. Chang, C.W. Hsia, W.C. Huang, T. Jayakumar, C.H. Hsia, T.L. Yen, J.R. Sheu, S. M. Hou, Myricetin as a promising inhibitor of platelet fibrinogen receptor in humans, Heliyon 9 (10) (2023) e20286.
[82] X. Song, H. Rao, C. Guo, B. Yang, Y. Ren, M. Wang, Y. Li, Z. Cao, J. Pei, Myricetin exhibit selective anti-lymphoma activity by targeting BTK and is effective via oral administration in vivo, Phytomedicine 93 (2021) 153802.
[83] S. Wegmann, J. Biernat, E. Mandelkow, A current view on Tau protein phosphorylation in Alzheimer's disease, Curr. Opin. Neurobiol. 69 (2021) 131–138.
[84] S. Mondragón-Rodríguez, G. Perry, J. Luna-Muñoz, M.C. Acevedo-Aquino, S. Williams, Phosphorylation of tau protein at sites Ser(396-404) is one of the earliest events in Alzheimer's disease and Down syndrome, Neuropathol. Appl. Neurobiol. 40 (2) (2014) 121–135.
[85] U. Sengupta, R. Kayed, Amyloid β, Tau, and α-Synuclein aggregates in the pathogenesis, prognosis, and therapeutics for neurodegenerative diseases, Prog. Neurobiol. 214 (2022) 102270.